the conjugation of proteins to poly(ethylene glycol) (PEG) [10–20]. PEG-modified proteins have lower clearance rates from blood circulation and show reduce immunogenicity in vivo, due to an increase in the proteins molecular weight and steric hindrance. Recently, several PEG-modified enzymes and proteins, such as PEG-modified uricase [17], L-asparaginase [18], interleukin 2 [19], superoxide dismutase [20], and interferon [14] have been undergoing clinical trials. PEG-modified adenosine deaminase has been filed with the FDA and is used to treat patients diagnosed with adenosine deaminase-deficient severe combined immunodeficiency syndrome [15]. However, it has been reported that the PEG-modified proteins mainly distribute in the blood, suggesting that their transport from blood to cells or tissues is unlikely. Recently studies using polymer-modified drug designs have focused on site-specific targeting of specified organs, tissues and cells, in addition to prolonged blood circulation, reduced immunogenicity and antigenicity. For polymer-modified drugs, which are particularly applicable to cardiovascular diseases, selective control of distribution or localization is of primary interest.

Control of the interaction between water-soluble polymers and cell membranes may provide a means for designing polymer-modified drugs with selective distribution and localization characteristics. In this study, we designed new water-soluble polymers as polymeric modifiers for drugs. These water-soluble polymers possess triphenylmethane leucohydroxide groups, which dissociate into triphenylmethyl cations and counter hydroxide ions upon UV irradiation (Scheme 1). The preparation and purification of the photodissociable polymers is quite simple and reliable. It was expected that under conditions where the photo-dissociable polymer is not irradiated the modified drug would reside mainly in the blood due to the nonionic nature of the photodissociable polymer. In contrast, irradiation of the modified drug could potentially facilitate enhanced residence on the cellular surfaces due to the generation of a cationic nature to the polymer. Such sequential stimulation may facilitate the transmembrane transport of the modified drug, whereas stronger irradiation may drive intracellular transport or cause cell damage.

As shown in Fig. 1, irradiation of the aqueous solution of the photodissociable polymer **2** resulted in the solution changing immediately from neutral to basic and was ascribed to the photo-dissociation of the leucohydroxide moiety, generating a triphenylmethy cation and hydroxide ion. By using the absorption coefficient of triphenylmethane leucohydroxide, which dissociates completely into an ion pair under acidic conditions, about 90% of the triphenylmethane leucohydroxide group of the polymer **2** dissociated into an ion pair after 5 min of irradiation.

Using the prepared photo-cation generatable polymer **2**, control of the nature and magnitude of the interaction with the cells was performed and assessed using a calcium ion-sensitive photoprotein, aequorin, which can bind three calcium ions per molecule accompanying with emission of chemiluminescence. The intensity of the emission is proportion to $[Ca^{2+}]^{1/2.5}$, which was experimentally confirmed by Prendergast and co-workers [34] It was thought that quantitative measurement of the cytosolic calcium ion concentration, and its time-dependent change, may enable predictions to be made regarding the distribution and localization of the drugs modified with the water-soluble photodissociable polymer. We used endothelial cells, which are one of anchorage-dependent cells. Such cells are =exhibited particular properties after adhering on a substrate. In this study, we measured interaction between cell membranes and polymers, which may be non-biospecific and may not be dependent on the particular properties of endothelial cells. Therefore, the interaction can be measured even under suspension condition.

As expected, the cationic polymer, derived from the photo-cation generatable polymer **2** upon UV irradiation, induced an inflow of calcium ions into endothelial cells, resulting in an elevation of cytosolic calcium ions, whilst no measurable inflow was observed for the non-irradiated neutral polymer. A longer irradiation time, and a higher content of the photodissociable group resulted in a greater inflow of calcium ions. On the other hand, no calcium ion inflow was observed by the elevation of pH to about 9 with the addition of an alkaline solution. Therefore, it can be said that the inflow of the calcium ions may be occurred by non-biospecific membrane stimulation not by biospecific mechanism such as calcium ion channels, indicating the amount of the calcium ion inflow may be corresponding to the magnitude of

the membrane stimulation by the direct interaction between cell membranes and polymers. Using the developed photo-cation generatable copolymers, the interaction between cells and water-soluble polymers could be controlled by the irradiation time, and composition and amount of the water-soluble polymers. As shown in Fig. 3, the cytosolic calcium ion concentration increased to a maximum at a polymer concentration of 10 mg/ml and thereafter was constant with higher polymer concentrations. This dependence suggests that the polymer may induce two competitive processes during stimulation. In the case of the 20 and 30 mg/ml concentrations of polymer **2a**, shortening the time before the addition of Triton X-100 led to greater luminescence using the prescribed experimental conditions. In both concentrations, when Triton X-100 was added to the cell suspension 1-min after the addition of polymer **2a** the magnitude of Triton X-100-induced chemiluminescence increased by about 1.2 times of that obtained 5 min after the polymer addition. In contrast, at the concentration of 10 mg/ml there was little different on the magnitude of the interaction by changing the time of the addition of Triton X-100. These indicated that at higher concentrations a weak continuous stimulation of cell membranes, in addition to an immediate transient stimulation, might be occurring. The mechanism for the $Ca^{2+}$ elevation is not well understood, but at higher concentrations of the photodissociable polymer longer lasting stimulation may occur due to the continuous stimulation induced by association with the membrane surface.

As demonstrated in Table 3, even at total concentrations of 10 mg/ml, the photodissociable polymer **2a**, caused little cellular damage with the exclusion of trypan blue regardless of the presence of UV irradiation. The growth of the ECs, treated with UV irradiated polymers, was little different to that of the control. It was of interest, however, that after treatment with the UV-irradiated polymer **2a**, which has a smaller content of the photo-dissociable group, the copolymer, which has a fluorescent triphenylmethane leucohydroxide group, was taken up by the cells as observed using fluorescent microscopy. The typical fluorescence micrograph of endothelial cells immediately after the treatment with copolymer **2a** pre-irradiated for 5 min at the total concentration of 10 mg/ml was shown in Fig. 6. Fluorescence was

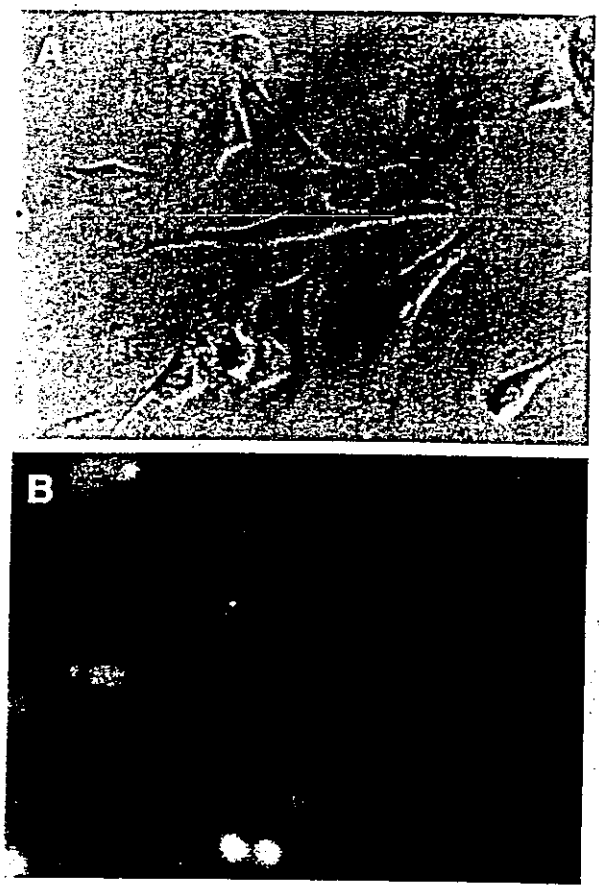


Fig. 6. Phase contrast micrograph (A) and fluorescence micrograph (B) of endothelial cells immediately after treatment with a PBS solution of copolymer **2b** (concentration; 10 mg/ml) pre-irradiated for 5 min.

observed only at the cells adhered. This may be due to the transmembrane transport of the copolymer into cells, which is associated with the fact that cationic peptides such as poly-L-lysine are taken up by cells [35]. Thus, this photo-cation generatable copolymer is expected to enhance the residency on the EC surface and may facilitate the transmembrane transport of the polymer-modified drug. On the other hand, treatment with photoirradiated polymer **2b**, which has a larger content of the photo-dissociable group, indicated that the growth of the ECs was dose-dependently inhibited. The stronger cationic polymers may disturb the membrane, resulting in cell death or penetration/transport of the polymers themselves.

## 5. Conclusion

The nature and magnitude of the interaction between photo-cation generatable water-soluble copolymers and ECs can be controlled by UV irradiation condition in addition to composition and amount of the copolymer. Changes in irradiation time, concentration of the photo-cation generatable copolymer and the density of the photodissociable group in the polymer may be used to design hybrid drugs with selective distribution and location characteristics. Such tailor-made hybrid drugs may provide a powerful therapeutic tool for the treatment of cardiovascular diseases.

## Acknowledgements

The authors thank Dr. Yasuo Tsutsumi (Osaka University) for fruitful advice and discussion. This study was supported by 'Research Grants for Advanced Medical Technology', 'Human Genome, Tissue Engineering and Food Biotechnology', and 'Aging and Health' from the Ministry of Health, Labour and Welfare of Japan, and by Grant-in-Aid for Scientific Research (B2-13450302, 2-14030095) from the Ministry of Education, Science, Sports and Culture of Japan.

## References

[1] Y. Kojima, A. Haruta, T. Imai, M. Otagiri, H. Maeda, Conjugation of Cu,Zn-superoxide dismutase with succinylated gelatin: pharmacological activity and cell-lubricating function, Bioconjug. Chem. 4 (1993) 490–498.

[2] K. Wong, L.G. Cleland, M.J. Poznansky, Enhanced anti-inflammatory effect and reduced immunogenicity of bovine liver superoxide dismutase by conjugation with homologous albumin, Agents Actions 10 (1980) 231–239.

[3] U. Wulbrand, M. Feldman, A. Pfestroff, H.C. Fehman, J. Du, J. Hiltunen, M. Marquez, R. Arnold, J.E. Westlin, S. Nilsson, A.R. Holmberg, A novel somatostatin conjugate with a high affinity to all five somatostatin receptor subtypes, Cancer 94 (2002) 1293–1297.

[4] K. Sakurai, K. Miyazaki, Y. Kodera, H. Nishimura, M. Shingu, Y. Inada, Anti-inflammatory activity of superoxide dismutase conjugated with sodium hyaluronate, Glycoconj. J. 14 (1997) 723–728.

[5] W. Mier, R. Eritja, A. Mohammed, U. Haberkorn, M. Eisenhut, Preparation and evaluation of tumor-targeting peptide-oligonucleotide conjugates, Bioconjug. Chem. 11 (2000) 855–860.

[6] A. Astriab-Fisher, D.S. Sergueev, M. Fisher, B.R. Shaw, R.L. Juliano, Antisense inhibition of P-glycoprotein expression using peptide-oligonucleotide conjugates, Biochem. Pharmacol. 60 (2000) 83–90.

[7] P. Caliceti, O. Schiavon, F.M. Veronese, Immunological properties of uricase conjugated to neutral soluble polymers, Bioconj. Chem. 12 (2001) 515–522.

[8] Y. Mu, H. Kamada, H. Kodaira, K. Sato, Y. Tsutsumi, M. Maeda, K. Kawasaki, M. Nomizu, Y. Yamada, T. Mayumi, Bioconjugation of laminin-related peptide YIGSR with polyvinyl pyrrolidone increases its antimetastatic effect due to a longer plasma half-life, Biochem. Biophys. Res. Commun. 264 (1999) 763–767.

[9] E. Ranucci, G. Spagnoli, P. Ferruti, D. Sgouras, R. Duncan, Poly(amidoamine)s with potential as drug carriers: degradation and cellular toxicity, J. Biomater. Sci. Polym. Ed. 2 (1991) 303–315.

[10] G. Molineux, Pegylation: engineering improved pharmaceuticals for enhanced therapy, Cancer Treat. Rev. 28 (Suppl. A) (2002) 13–16.

[11] R.M. Bukowski, C. Tendler, D. Cutler, E. Rose, M.M. Laughlin, P. Statkevich, Treating cancer with PEG Intron: pharmacokinetic profile and dosing guidelines for an improved interferon-alpha-2b formulation, Cancer 95 (2002) 389–396.

[12] H. Sato, Enzymatic procedure for site-specific pegylation of proteins, Adv. Drug Deliv. Rev. 54 (2002) 487–504.

[13] M.J. Roberts, M.D. Bentley, J.M. Harris, Chemistry for peptide and protein PEGylation, Adv. Drug Deliv. Rev. 54 (2002) 459–476.

[14] Y.S. Wang, S. Youngster, M. Grace, J. Bausch, R. Bordens, D.F. Wyss, Structural and biological characterization of pegylated recombinant interferon alpha-2b and its therapeutic implications, Adv. Drug Deliv. Rev. 54 (2002) 547–570.

[15] M.S. Hershfield, Adenosine deaminase deficiency: clinical expression, molecular basis, and therapy, Semin. Hematol. 35 (1998) 291–298.

[16] N.N. Sanders, S.C. De Smedt, S.H. Cheng, J. Demeester, Pegylated GL67 lipoplexes retain their gene transfection activity after exposure to components of CF mucus, Gene Ther. 9 (2002) 363–371.

[17] C.C. Chua, M.L. Greenberg, A.T. Viau, M. Nucci, W.D. Brenckman Jr., M.S. Hershfield, Use of polyethylene glycol-modified uricase (PEG-uricase) to treat hyperuricemia in a patient with non-Hodgkin lymphoma, Ann. Intern. Med. 109 (1988) 114–117.

[18] C.W. Taylor, R.T. Dorr, P. Fanta, E.M. Hersh, S.E. Salmon, A phase I and pharmacodynamic evaluation of polyethylene glycol-conjugated L-asparaginase in patients with advanced solid tumors, Cancer Chemother. Pharmacol. 47 (2001) 83–88.

[19] B. Kaplan, R.L. Moy, Effect of perilesional injections of PEG-interleukin-2 on basal cell carcinoma, Dermatol. Surg. 26 (2000) 1037–1040.

[20] J.P. Muizelaar, Clinical trials with Dismutec (pegorgotein; polyethylene glycol-conjugated superoxide dismutase; PEG-

SOD) in the treatment of severe closed head injury, Adv. Exp. Med. Biol. 366 (1994) 389–400.
[21] Y. Mu, H. Kamada, Y. Kaneda, Y. Yamamoto, H. Kodaira, S. Tsunoda, Y. Tsutsumi, M. Maeda, K. Kawasaki, M. Nomizu, Y. Yamada, T. Mayumi, Bioconjugation of laminin peptide YIGSR with poly(styrene co-maleic acid) increases its antimetastatic effect on lung metastasis of B16-BL6 melanoma cells, Biochem. Biophys. Res. Commun. 255 (1999) 75–79.
[22] Y. Tsutsumi, T. Matsuda, T. Mayumi, Fundamental study on hybrid drug design: interaction of water-soluble polymers with endothelial cells by means of cytosolic calcium ion mobilization (in preparation).
[23] T. Kojima, M. Hashida, S. Muranishi, H. Sezaki, Mitomycin C-dextran conjugate: a novel high molecular weight pro-drug of mitomycin C, J. Pharm. Pharmacol. 32 (1980) 30–34.
[24] H. Sezaki, M. Hashida, Macromolecule-drug conjugates in targeted cancer chemotherapy, Crit. Rev. Ther. Drug Carrier. Syst. 1 (1984) 1–38.
[25] P.C. Johnson, J.A. Ware, P.B. Cliveden, M. Smith, A.M. Dvorak, E.W. Salzman, Measurement of ionized calcium in blood platelets with the photoprotein aequorin. Comparison with Quin 2, J. Biol. Chem. 260 (1985) 2069–2076.
[26] T. Lecompte, F. Potevin, P. Champeix, M.C. Morel, R. Favier, M.F. Hurtaud, N. Schlegel, M. Samama, C. Kaplan, Aequorin-detected calcium changes in stimulated thrombasthenic platelets. Aggregation-dependent calcium movement in response to ADP, Thromb. Res. 58 (1990) 561–570.
[27] O. Shimomura, F.H. Johnson, Properties of the bioluminescent protein aequorin, Biochemistry 8 (1969) 3991–3997.
[28] O. Shimomura, F.H. Johnson, Calcium binding, quantum yield, and emitting molecule in aequorin bioluminescence, Nature 227 (1970) 1356–1357.
[29] R.C. Bertelson, in: G.H. Brown (Ed.), Photochromism. Techniques of Chemistry, Vol. III, Wiley-Interscience, New York, 1971, p. 294.
[30] M. Irie, D. Kungwatchakun, Reversible photostimulated dilation of polyacrylamide gels having triphenylmethane leucoderivatives, Macromolecules 19 (1986) 2476.
[31] A. Yamaguchi, H. Suzuki, K. Tanoue, H. Yamazaki, Simple method of aequorin loading into platelets using dimethyl sulfoxide, Throrub. Res. 44 (1986) 165–174.
[32] F. Medzihradsky, M.J. Marks, Measures of viability in isolated cells, Biochem. Med. 13 (1975) 164–177.
[33] M.I. Aveldano, R.S. Diaz, P. Regueiro, J. Monreal, Solubilization of myelin membranes by detergents, J. Neurochem. 57 (1991) 250–257.
[34] D.G. Allen, J.R. Blinks, F.G. Prendergast, Aequorin luminescence: relation of light emission to calcium concentration: a calcium-independent component, Science 195 (1977) 996–998.
[35] H.J. Ryser, Uptake of protein by mammalian cells: an underdeveloped area. The penetration of foreign proteins into mammalian cells can be measured and their functions explored, Science 159 (1968) 390–396.

Photochemistry and Photobiology, 2003, 77(5): 480–486

# Photocontrol of Cell Adhesion and Proliferation by a Photoinduced Cationic Polymer Surface¶

Yasuhide Nakayama*[1], Akiko Furumoto[1], Satoru Kidoaki[2] and Takehisa Matsuda*[2]

[1]Department of Bioengineering, National Cardiovascular Center Research Institute, Osaka, Japan and
[2]Department of Biomedical Engineering, Graduate School of Medicine, Kyushu University, Fukuoka, Japan

Received 15 October 2002; accepted 20 February 2003

## ABSTRACT

**In this study photoinduced cation generation, based on the photochemical properties of malachite green (MG), was used for the surface design and *in vitro* photochemical control of cell adhesion and proliferation. The MG-derivatized surface was prepared by coating a photoreactive polymer as a substrate onto a poly(ethylene terephthalate) (PET) sheet. The photoreactive polymer was radical copolymer of styrene with the MG-derivatized monomer diphenyl(4-vinylphenyl)methane leucohydroxide (degree of substitution of MG unit: 12.4 mol%). Water contact angle measurements and X-ray photoelectron spectroscopy revealed high hydrophobicity and homogeneous distribution of the MG groups on the outermost surface of the coated film, respectively. When the coated film was exposed to ultraviolet light (UV) irradiation at wavelengths of 290–410 nm, a time-dependent color change of the film was observed from pale yellow, before irradiation, to green. These results indicated generation of cations on the film surface by photochemical cation generation of the MG groups, which was quantitatively characterized by force *versus* distance curves measurements in atomic force microscopic (AFM) observation using a carboxylated AFM tip. The seeding and culture of endothelial cells showed a marked reduction in adhesion on the nonirradiated coated film surface, whereas the UV-irradiated surface promoted cell adhesion and proliferation except for incubation in serum-free medium, which was similar to commercial tissue culture PET sheet. These observations may be due to adsorption of cell adhesive proteins, typified by fibronectin, in serum-containing medium onto the cationized photoreactive copolymer surface by electrostatic interactions.**

## INTRODUCTION

Studies to examine the induction of cell movement, direction and organization, together with the role of cell function (attachment–adhesion, elongation, migration and proliferation) on cell morphology have been demonstrated using micropatterned surfaces. These surfaces enable adhesion and nonadhesion areas of cells to be precisely segregated at the micrometer level (1–18). Such micropatterned surfaces can be produced using various existing microprocessing techniques such as photolithography using conventional semiconductor manufacturing techniques (1,9,11, 15) or by combining photolithography with silane coupling on a glass surface (2–4,10). In addition, regional ultraviolet light (UV) irradiation (16) including an excimer laser (17), which has been used in recent years for manufacturing of super high–density large-scale integration circuits, realized submicrometer-order precision. On the other hand, microcontact printing, which combines a microprocessed stamp with an alkanethiol ink that can form a self-assembly monolayer on gold surface (5,6), has recently been developed and allows the production of precise micropatterned surfaces using very simple procedures (13,18).

We have previously developed photochemical driven surface modification methods. These include photograft polymerization (7,8,19) using the photochemistry of dithiocarbamate, an "iniferter" (20–23), which acts as a radical polymerization initiator, transfer agent and terminator and photografting using photoreactive polymers derivatized with photoreactive groups (azide [1,11], dithiocarbamate [24] and benzophenone [25] groups generating radicals or coumarin [26] and cinnamate [27] groups showing dimerization). Using the surface graft polymerization method, micropatterned surfaces of polymers with multiply different physicochemical properties can be easily produced by regional photoirradiation in a particular monomer solution while moving the irradiation portion (8). Because cell adhesion and proliferation are enhanced on relatively hydrophobic or ionic (especially cationic) hydrophilic surface (28–31) via preadsorption of cell adhesive proteins such as fibronectin, vitronectin and lamimin in serum-containing medium onto the surfaces, it is possible that two-dimensionally patterned tissues could be readily produced that posses micrometer-order precision.

The next stage in preparing high-performance surfaces for cellular matrixes requires the development of technologies, which can reversibly control cell attachment and detachment or control direction of cell migration for *in situ* design of organization of adhered cells. A reversible cell attachment–detachment matrix was previously prepared using thermoinsolubilization of

¶Posted on the website on 6 March 2003.

*To whom correspondence should be addressed at: Department of Bioengineering, National Cardiovascular Center Research Institute, 5-7-1 Fujishiro-dai, Suita, Osaka 565-8565, Japan. Fax: 816-6872-8090; e-mail: nakayama@ri.ncvc.go.jp

*Department of Biomedical Engineering, Graduate School of Medicine, Kyushu University, 3-1-1 Maidashi, Higashi-Ku, Fukuoka 812-8582, Japan. Fax: 8192-642-6212; e-mail: matsuda@med.kyushu-u.ac.jp

*Abbreviations:* AFM, atomic force microscopic; AIBN, 2,2'-azobis(isobutyronitrile); EC, endothelial cells; f-d, force *versus* distance; GPC, gel permeation chromatography; MG, malachite green; NMR, nuclear magnetic resonance; PET, poly(ethylene terephthalate); PST, polystyrene; ST, styrene; UV, ultraviolet light; XPS, X-ray photoelectron spectroscopy.

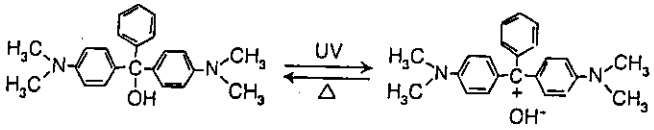

Figure 1. Photochemical dissociation into ion pairs of triphenylmethane leucohydroxide (MG).

poly(*N*-isopropylacryamide) for culture plate (32). However, the thermal reaction has met little regional control in principle because of an accompaniment of diffusion process. On the other hand, there is no report about *in situ* control of direction of cell migration.

The aim of this study was to develop a novel surface modification method, which can photochemically control cell attachment regions, as a fundamental base for *in situ* control of cell organization. To achieve this, a photochemical cation-generatable surface was designed based on the photochemistry of malachite green (MG). MG is a well-known photochromic molecule that reversibly dissociates into ion pairs under UV irradiation (33,34), producing intensely deep-green–colored triphenylmethyl cation, which is a plane structure, and counter hydroxide ions very rapidly (within 40 ns) and in high quantum yields (34), as shown in Fig. 1. We have previously synthesized water-soluble polyacrylamide copolymers with MG side chains (35). Using this system we found that a cationic copolymer, produced by UV irradiation, induced an immediate strong interaction with cells suspended in buffer solution and was dependent on irradiation time, concentration of copolymer and content of MG groups. Therefore, using the photochemistry of MG, which can reversibly generate the cation, *in situ* control of the direction of cell migration will be realized by moving the irradiation portion.

In this study a hydrophobic MG-derivatized copolymer composed mainly of styrene (ST) units was prepared and used as a photoreactive polymer. UV irradiation–induced changes on the surface physicochemical properties of the photoreactive copolymer film were evaluated by X-ray photoelectron spectroscopy (XPS), water contact angle measurements and atomic force microscopic (AFM) analyses. Using this novel surface an initial study in *in vitro* photochemical control of cell adhesion and proliferation was performed.

## MATERIALS AND METHODS

*Materials.* ST was obtained from Ohken Co., Ltd. (Tokyo, Japan). All solvents and reagents were of special reagent grade and were purchased from Wako Pure Chemical Industries, Ltd. (Osaka, Japan) and used after standard purification. 2,2′-Azobis(isobutyronitrile) (AIBN) was recrystallized twice from methanol.

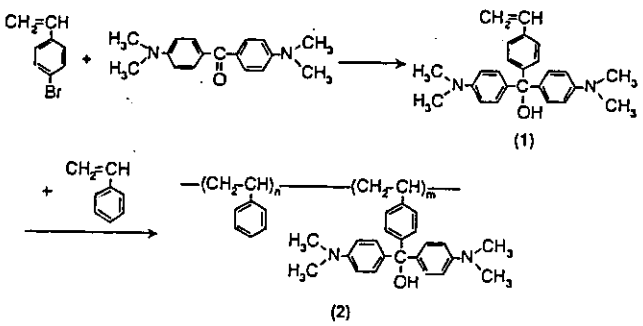

Figure 2. Synthetic route for the preparation of photoreactive copolymer (2) with MG groups.

Table 1. Preparation of poly(styrene-co-diphenyl(4-vinylphenyl)methane leucohydroxide) (2)*

| Monomer feed ratio (mol%) | | Copolymer (2) | | |
|---|---|---|---|---|
| ST | (1) | Conversion (%) | Mn† ($\times 10^4$ g/mol) | Content of (1) unit‡ (mol%) |
| 76 | 24 | 20 | 7.4 | 12.4 |

*Total monomer concentration = 200 mg/mL in benzene; initiator concentration = [monomer]/[initiator] = 100, 60°C, 18 h in sealed tubes.
†Determined by GPC measurements (calibrated with polystyrene); eluent, *N,N*-dimethylformamide.
‡Determined by $^1$H-NMR analyses.

*Preparation of the photoreactive polymer (2) and its film.* A glass tube containing a mixture of ST (447 mg, 4.3 mmol), diphenyl(4-vinylphenyl)-methane leucohydroxide (34) (1, 537 mg, 1.5 mmol), AIBN (9.5 mg, $5.8 \times 10^{-2}$ mmol; molar ratio of [monomer]/[initiator] = 100) and benzene (5 mL) was sealed under reduced pressure after three freeze–pump–thaw cycles for degassing. Polymerization was carried out for 18 h at 60°C in the dark. The polymer, after precipitation with a large amount of methanol, was filtered (11G4, TOP, Kyoto, Japan). Reprecipitation was carried out by exchanging benzene solution three times with methanol. The final precipitation was dried under a vacuum and stored in a dark desiccator, and the yield was 212 mg (20%). The molecular weight of the copolymer (2), estimated by gel permeation chromatography (GPC) analyses, was approximately $7.4 \times 10^4$g/mol. The content of the triphenylmethane leucohydroxide unit in the copolymer was 12.4 mol%, which was determined by $^1$H–nuclear magnetic resonance (NMR) spectroscopy.

Films of the photoreactive copolymer (2) were prepared by coating from the benzene solution (1% wt/vol, 100 μL per 1.5 $cm^2$) onto the circular poly(ethylene terephthalate) (PET) sheet (diameter: 14 mm, WAKO Plastic Sheet, Osaka, Japan) and air-dried.

*UV irradiation.* UV irradiation was carried out with an ultrahigh-pressure mercury-vapor lamp (250 W, SPOT CURE250, Ushio, Tokyo, Japan) through a quartz optical fiber (diameter: 5 mm, length: 1 m). The light wavelength (290 nm $< \lambda <$ 410 nm) was selected with the aid of cutoff filters (UV-D25 and UV-31, Toshiba, Tokyo, Japan). The light intensity, measured with a photometer (UVR-1, Topcon, Tokyo, Japan), was 0.5 mW/$cm^2$ at the sample surface.

*Surface characterization.* The chemical composition of the outermost surface layer of the MG-derivatized copolymer (2) film was determined by XPS (36,37) (ESCA 750, Shimadzu, Kyoto, Japan) using a magnesium anode (MgKα radiation) connected to a data processor ESCAPAC-760 at room temperature and $2 \times 10^{-7}$ Torr (8 kV, 20 mA) at a takeoff angle of 90°. The angle was defined as the angle between the sample surface and the electron optics of the energy analyzer. Because the elemental analysis data determined by XPS measurement were reproducible ($n = 3$, SD < 10%), only the average values were reported.

The surface wettability was evaluated by water contact angle measurements (38,39) using the sessile drop technique with a contact angle meter (CA-D, Kyowa Kaimenkagaku Co., Ltd., Tokyo, Japan).

Adhesion forces were determined from force *versus* distance (f-d) curve measurements obtained by AFM (40,41) (Dimension 3000, Digital Instruments, Santa Barbara, CA), using a probe-tip surface modified with a carboxyl group. This was prepared through self-assembled monolayer formation of 12-mercapto-1-dodecanoic acid, according to the method of our previous study (42). Thirty f-d curves were obtained at one location through repeated tip approach–retract cycles, and the measurements were then repeated at five locations for each sample. The frequency of the approach–retract cycle, 3.2 Hz, was chosen to minimize the noise fluctuation in a single f-d curve. Sequential f-d curves were collected using computer software at 1 s intervals. The adhesion force between the tip and the photoreactive copolymer film surface was evaluated from the hysteresis in the retract trace of the f-d curves, where the jump-height from the bottom of the retrace line corresponded to the total adhesive force strength. The spring constant (0.12 N/m), provided by the probe manufacturer (DNP-S, Digital Instruments), was used without further calibration in this study.

*Other physical measurements.* Average molecular weights were determined by GPC analyses (43,44) of *N,N*-dimethylformamide with a RI-

Table 2. Water contact angles and surface chemical compositions of the photoreactive copolymer film before and after UV irradiation

| Surface | Contact angle (°)* | | Element ratio† | |
|---|---|---|---|---|
| | Advancing | Receding | O/C | N/C |
| Nontreated PET | 74 ± 3.7 | 56 ± 2.1 | 0.43 (0.4)‡ | 0 (0)‡ |
| After coating of photoreactive copolymer (2) | | | | |
| without irradiation | 93 ± 2.1 | 89 ± 1.4 | 0.010 (0.012)‡ | 0.020 (0.025)‡ |
| with irradiation for 5 min | 73 ± 3.1 | 64 ± 5.2 | | |

*Measured by the sessile drop method (n = 5).
†Determined from XPS measurements (n = 3).
‡Parentheses show the theoretical values.

8012 instrument (Tosoh, Tokyo, Japan) at 40°C using Tosoh TSKgel α3000 and α6000 columns. The columns were calibrated using narrow weight distribution polystyrene (PST) standards. $^1$H-NMR spectra were obtained on a JEOL JNM-JX-270 (270 MHz) spectrometer (JEOL, Tokyo, Japan) and were recorded in dimethylsulfoxide-$d_6$ solutions using tetramethylsilane as the internal standard.

*Cell culture.* Endothelial cells (EC) harvested from bovine thoracic aorta by collagenase digestion were cultured in Dulbecco's modified Eagle's medium (Flow Laboratories, McLean, VA) supplemented with 15% fetal bovine serum (HyClone Laboratories, Inc., Logan, UT), a mixture of penicillin and streptomycin (50 mg/L, ICN Biomedicals Inc., Aurora, OH) and amphotericin B (2.5 mg/L, ICN Biomedicals Inc.). EC between the 14th and 16th passage were used. EC were seeded onto PET sheets (WAKO), placed at the bottom of PST 24 multiwell culture dishes (Corning, NY), with or without coating of the photoreactive copolymer at a density of $2 \times 10^4$ cells/well at 37°C in water saturated with 5% $CO_2$/95% air atmosphere for up to 3 days. Culture medium was replaced every day. Samples were observed by phase-contrast microscopy (Nikon Diaphoto, Tokyo, Japan) and photographed for at least three fields in each sample with a Nikon camera (HFX) using Polaroid 667 film (Polaroid, Cambridge, MA), and the number of adherent EC per unit area was counted.

## RESULTS AND DISCUSSION

### Surface preparation and characterization

The photoreactive copolymer (2) was prepared by radical copolymerization of ST with the MG-derivatized monomer dipheny (4-vinypheny)methane leucohydroxide (1), which was synthesized using the Grignared reaction with 4-bromostyrene and Michler's ketone (34), as shown in Fig. 2. The results of copolymerization are shown in Table 1, with the degree of substitution of the MG unit in the copolymer found to be 12.4 mol%.

The copolymer (2) was coated onto the surface of the PET sheet from its benzene solution to form a film. Water contact angle measurements of the film, when used as the base material, showed that both advancing and receding contact angles were significantly higher compared with the nontreated PET sheet. These results were similar to previously reported values for polystyrene (45) and showed high hydrophobicity (Table 2). Surface elemental analysis by XPS measurements revealed an oxygen/carbon (O/C) elemental ratio of 0.010 and a nitrogen/carbon (N/C) ratio of 0.021, which were close to their respective theoretical values of 0.012 for O/C and 0.025 for N/C as calculated from the chemical structure of the copolymer (Table 2). These results indicate that the MG groups were distributed on the outermost surface of the coating film according to the composition ratio of the copolymer (2).

When the coated film surface was UV irradiated for 5 min, the water contact angle decreased slightly (Table 2), indicating a slight increase in surface hydrophilicity. In addition the film, which was pale yellow color before irradiation, turned yellowish green (Fig. 3). With increasing irradiation time the depth of the green color increased and became almost constant after 20 min irradiation. These findings strongly suggest the generation of triphenylmethyl cations from the MG groups after UV irradiation, as shown in Fig. 1. The green color was maintained, without fading, for several days at 37°C, indicating that the generated cations were highly stable in the polymer matrix.

To quantitatively characterize the positive charge on the outermost surface of the photoreactive copolymer-coated films, which were induced by ionization of the MG on UV irradiation, AFM f-d curve measurements were performed for each surface before and after UV irradiation. For these measurements the AFM tip with close-packed carboxyl groups was used. Because the carboxylated tip is negatively charged under neutral pH, positive charges detected were from electrostatic attractive interactions between the surface and the negatively charged tip, as shown on the f-d curve profiles.

Figure 4 shows the representative f-d curves obtained for the photoreactive copolymer-coated surface before (Fig. 4A) and after (Fig. 4B) UV irradiation for 20 min. The approaching trace of the f-d curve (dashed curve in Fig. 4) obtained after UV irradiation showed a remarkable pull-in force, which was not seen before irradiation. In the retracting trace of the f-d curve (solid curve), the

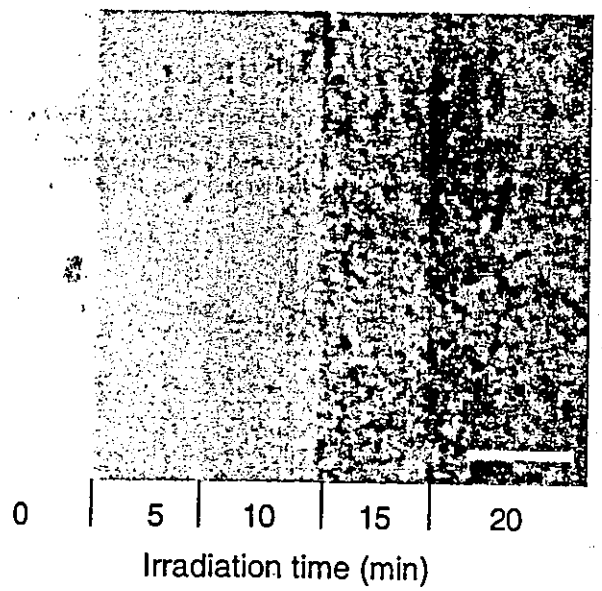


Figure 3. Color change of the photoreactive copolymer (2)-coated PET sheet using UV irradiation. Bar = 500 μm.

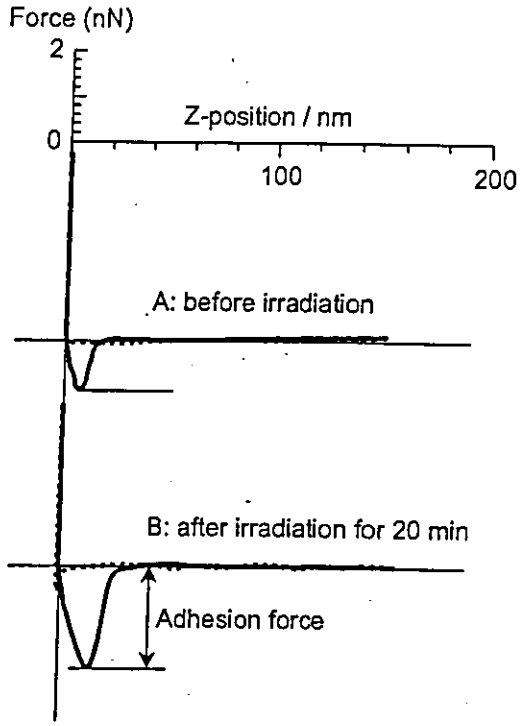


Figure 4. AFM force curves on the photoreactive copolymer (2) surface before (A) and after (B) UV irradiation for 20 min. Dashed curves: approaching trace. Solid curves: retracting trace. The zero position of the tip is expediently defined as the starting position of the linear part in the tip-surface contact region.

typical adhesive jump-height was larger on the surface after UV irradiation than before irradiation. Adhesion forces measured from 150 f-d curves ranged from 0.5 to 3.6 nN, as shown in the histograms in Fig. 5. The mean adhesion force appeared to be larger on the surface after UV irradiation ($2.0 \pm 0.7$ nN) than before irradiation ($1.3 \pm 0.4$ nN). Such an increase in adhesion force on the UV-irradiated surface is attributable to the contribution from the electrostatic-binding force at the interface between the negatively charged carboxylated tip and the positively charged photoreactive copolymer-coated surface. This in turn was added to the basal adhesive interaction between the tip and the surface before UV irradiation.

The above observations verify that the copolymer-coated surface was undoubtedly positively charged after UV irradiation. Because the adsorption force was markedly different among the measurement sites, the surface was considered to be heterogeneous in the microscopic range at the nanometer level. On the other hand, in water contact angle measurements, which have micrometer level precision corresponding to a cellular size, reproducible data were obtained with very small standard deviation, as shown in Table 2. Therefore, it can be said that the cations were uniformly produced on the photoreactive copolymer surface within a cellular size.

### Cellular responses

EC were seeded on the surface of the photoreactive copolymer films either with or without UV irradiation. After 3 h of incubation on the whole surface of the film, which was UV irradiated homogeneously for 20 min, the seeded cells adhered and elongated in a manner very similar to that on the surface of a PET tissue culture sheet that was used as the control (Fig. 6). In contrast, almost all

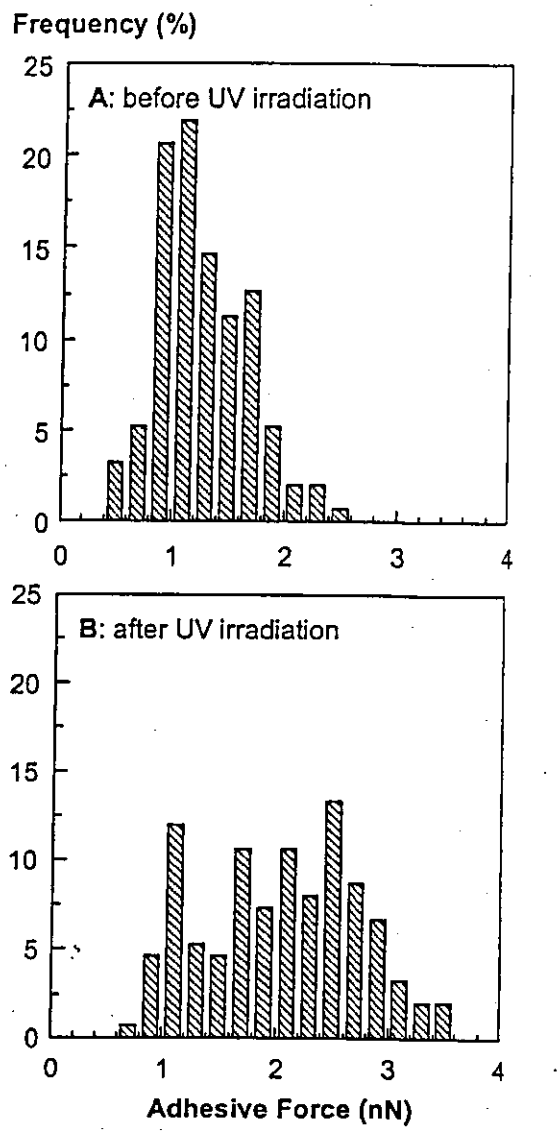


Figure 5. Histograms of the frequency of adhesion force observed in the repetitive f-d curve measurements between $COO^-$-AFM tip and the photoreactive copolymer-coated surfaces before (A) and after (B) UV irradiation for 20 min.

cells attached onto the nonirradiated film surface were circular in shape. With longer culture incubation, cells on the surface of the irradiated films proliferated with a doubling time of about 1 day, as did the control (Fig. 7). After 3 days of incubation the surface of the UV-irradiated film and the control surface were fully covered with a confluent monolayer of cells (Fig. 6). On the other hand, cells on the surface of the nonirradiated film showed little proliferation and negligible change in cell numbers even after 3 days of culture (Fig. 7). When the surface of the nonirradiated film was precoated with such cell adhesive proteins (fibronectin), the cells showed much adhesion and proliferation (Fig. 7).

It has been reported that cellular responses such as attachment–adhesion, spreading and proliferation on material surfaces are generally dependent on surface characteristics such as chemical composition and properties. In the cellular attachment–adhesion two distinctly different mechanisms have been discussed (28–31,46–54). One is biospecific interaction of cellular membrane receptors and adsorbed cell adhesive proteins, typified by fibro-

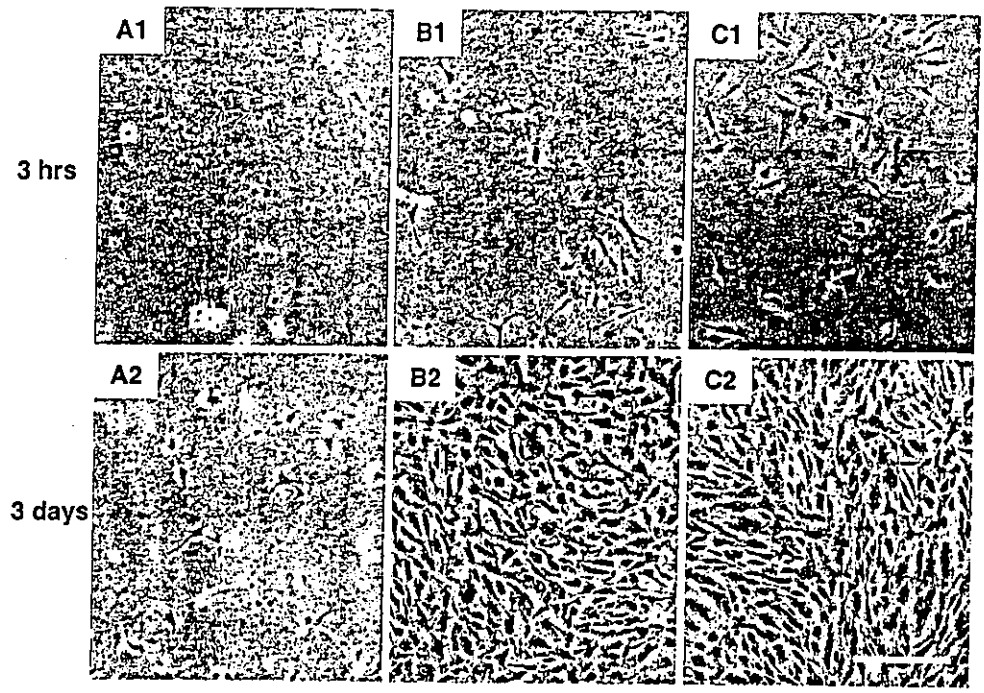


**Figure 6.** Phase-contrast micrographs of adhered EC on the photoreactive copolymer (2) film surface before (A) and after (B) UV irradiation for 20 min and tissue culture dish (C). Bar = 100 μm.

nectin and vitronectin (55–57). Such surfaces, in which adsorption of such adhesive proteins present in a serum-containing medium preferentially occur, are relatively hydrophobic or ionic (especially cationic). The other mechanism proceeded *via* direct interaction of negatively charged cellular membrane and cationically charged surfaces *via* electrostatic interactions, which occurred even under incubation in a serum-free medium. For examples, poly(L-lysine) or cationic synthetic polymer surfaces enhanced cellular adhesion (47–51). On the other hand, least protein adsorption and easiest desorptive surfaces have been identified as nonionic swellable or highly hydrophobic surfaces. In fact, poly(ethylene glycol)-derivatized surface or the fluorinated one reduced protein adsorption, and concomitantly, significant reduced attachment of platelets and EC were observed (58).

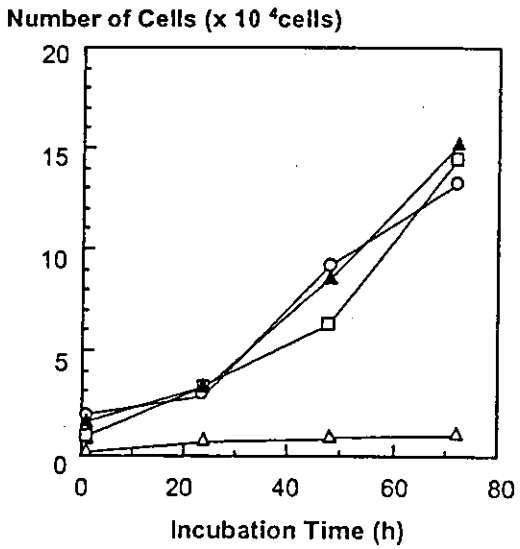


**Figure 7.** Growth curves of EC adhered on (○) tissue culture PET sheet, (△) nonirradiated photoreactive copolymer (2) film, (□) photoreactive copolymer (2) film UV irradiated for 20 min, (▲) nonirradiated photoreactive copolymer (2) film with coating of fibronectin and (●) photoreactive copolymer (2) film UV irradiated for 20 min under incubation in serum-free medium.

In this study, the UV-irradiated photoreactive copolymer film surface, where positive charges were homogeneously distributed all over the area in the precision at cellular level, enhanced cell adhesion and growth (Figs. 6 and 7). This observation is well correlated with data in previous studies reported from many institutions (46–54), whereas under incubation in the serum-free medium, attachment of cells was markedly prevented on the photoreactive copolymer film even after UV irradiation, as shown in Fig. 7. This phenomenon was observed under 3 h incubation in a saline solution (data not shown). These may be due to low density of the generated cationic charges. On the other hand, transformation of MG by UV irradiation forms planar structure in addition to carbocation. However, the structural change is hard to lead to any changes of the overall structure of the MG-derivatized copolymer because of random direction of the copolymer in addition to very low content of MG unit in the copolymer (*ca* 10%). Therefore, it is suggested that the enhancement of cell adhesion and proliferation was induced by adsorption of cell adhesive proteins in a serum-containing medium on the UV-irradiated cationized photoreactive copolymer surface by electrostatic interactions. In addition, it seems that protein adsorption alone was difficult to occur on the nonirradiated photoreactive copolymer surface, thereby inhibiting cell proliferation.

The results from this study suggest that UV irradiation provides proliferativity to cell nonproliferative surfaces and allows control of cell proliferation on the surface. When high-density cell adhesion areas are partially produced on a completely non-cell adhesive surface with regional precision, by controlling areas of irradiation and UV is irradiated on their adjacent nonirradiated areas, it is

possible to induce cell movement–proliferation in newly irradiated areas. On the other hand, it seems that the reversible control of cell attachment or detachment on culture surfaces may be realized by the hypothesis as follows. The transformation of MG is reversible in solution. If highly cationically charged graft surfaces induced from the MG-derivatized surface will enhance cellular attachment *via* electrostatic interaction with the negatively charged cellular membrane without adsorption of the cell adhesive proteins, cells will be attached to only limited areas under UV irradiation, whereas absence of the cationically charges, which may be induced by cessation of irradiation, may lead to detachment of the attached cells by disappearance of electrostatic interaction between the cell membrane and the substrate. These studies for *in situ* design of organization of adhered cells are currently in progress.

*Acknowledgements*—This work has been supported in part by "Research Grants for Advanced Medical Technology," "Human Genome, Tissue Engineering and Food Biotechnology" and "Aging and Health" from the Ministry of Health, Labour and Welfare of Japan and by Grant-in-Aid for Scientific Research (B2-13450302, 2-14030095) from the Ministry of Education, Science, Sports and Culture of Japan.

## REFERENCES

1. Sugawara, T. and T. Matsuda (1995) Photochemical surface derivatization of a peptide containing Arg-Gly-Asp (RGD). *J. Biomed. Mater. Res.* **29**, 1047–1052.
2. Healy, K. E., C. H. Thomas, A. Rezania, J. E. Kim, P. J. McKeown, B. Lom and P. E. Hockberger (1996) Kinetics of bone cell organization and mineralization on materials with patterned surface chemistry. *Biomaterials* **17**, 195–208.
3. Lom, B., K. E. Healy and P. E. Hockberger (1993) A versatile technique for patterning biomolecules onto glass coverslips. *J. Neurosci. Methods* **50**, 385–397.
4. Britland, S., P. Clark, P. Connolly and G. Moores (1992) Micropatterned substratum adhesiveness: a model for morphogenetic cues controlling cell behavior. *Exp. Cell Res.* **198**, 124–129.
5. Lopez, G. P., M. W. Albers, S. L. Schreiber, R. Carroll, E. Peratta and G. M. Whitesides (1993) Convenient methods for patterning the adhesion of mammalian cells to surfaces using self-assembled monolayers of alkanethiolates on gold. *J. Am. Chem. Soc.* **115**, 5877–5878.
6. Singhvi, R., A. Kumar, G. P. Lopez, G. N. Stephanopoulos, D. I. Wang, G. M. Whitesides and D. E. Ingber (1994) Engineering cell shape and function. *Science* **264**, 696–698.
7. Nakayama, Y. and T. Matsuda (1996) Surface macromolecular architectural designs using photo-graft copolymerization based on photochemistry of benzyl *N,N*-diethyldithiocarbamate. *Macromolecules* **29**, 8622–8630.
8. Higashi, J., Y. Nakayama, R. E. Marchant and T. Matsuda (1999) High-spatioresolved microarchitectural surface prepared by photograft copolymerization using dithiocarbamate: surface preparation and cellular responses. *Langmuir* **15**, 2080–2088.
9. Soekarno, A., B. Lom and P. E. Hockberger (1993) Pathfinding by neuroblastoma cells in culture is directed by preferential adhesion to positively charged surfaces. *Neuroimage* **1**, 129–144.
10. Kleinfeld, D., K. H. Kahler and P. E. Hockberger (1988) Controlled outgrowth of dissociated neurons on patterned substrates. *J. Neurosci.* **8**, 4098–4120.
11. Matsuda, T. and T. Sugawara (1996) Control of cell adhesion, migration, and orientation on photochemically microprocessed surfaces. *J. Biomed. Mater. Res.* **32**, 165–173.
12. Folkman, J. and A. Moscona (1978) Role of cell shape in growth control. *Nature* **273**, 345–349.
13. Chen, C. S., M. Mrksich, S. Huang, G. M. Whitesides and D. E. Ingber (1997) Geometric control of cell life and death. *Science* **276**, 1425–1428.
14. Opas, M. (1989) Expression of the differentiated phenotype by epithelial cells in vitro is regulated by both biochemistry and mechanics of the substratum. *Dev. Biol.* **131**, 281–293.
15. Bhatia, S. N., M. L. Yarmush and M. Toner (1997) Controlling cell interactions by micropatterning in co-cultures: hepatocytes and 3T3 fibroblasts. *J. Biomed. Mater. Res.* **34**, 189–199.
16. Hammarback, J. A., S. L. Palm, L. T. Furcht and P. C. Letouneau (1985) Guidance of neurite outgrowth by pathways of substratum-adsorbed laminin. *J. Neurosci. Res.* **13**, 213–220.
17. Nakayama, Y. and T. Matsuda (1996) Excimer laser-induced surface fixation of polymer and its patterning. *J. Appl. Phys.* **80**, 505–508.
18. Kumar, A. and G. E. Whitesides (1994) Patterned condensation figures as optical diffraction gratings. *Science* **263**, 60–63.
19. Brodbeck, W. G., J. Patel, G. Voskerician, E. Christenson, M. S. Shive, Y. Nakayama, T. Matsuda, N. P. Ziats and J. M. Anderson (2002) Biomaterial adherent macrophage apoptosis is increased by hydrophilic and anionic substrates *in vivo*. *Proc. Natl. Acad. Sci. USA* **99**(16), 10287–10292.
20. Otsu, T. and M. Yoshida (1982) Role of initiator-transfer agent-terminator (iniferter) in radical polymerizations: polymer design by organic disulfides as iniferters. *Makromol. Chem. Rapid Commun.* **3**(2), 127–132.
21. Otsu, T., M. Yoshida and T. Tazaki (1982) A model for living radical polymerization. *Makromol. Chem. Rapid Commun.* **3**(2), 133–140.
22. Otsu, T., T. Matsunaga, T. Doi and A. Matsumoto (1995) Features of living radical polymerization of vinyl monomers in homogeneous system using *N,N*-diethyldithiocarbamate derivatives as photoiniferters. *Eur. Polym. J.* **31**(1), 67–78.
23. Otsu, T. (2000) Iniferter concept and living radical polymerization. *J. Polym. Sci. Part A: Polym. Chem.* **38**(12), 2121–2136.
24. Nakayama, Y., M. Takatsuka and T. Matsuda (1996) Surface hydrogelation using photolysis of dithiocarbamate or xanthate: hydrogelation, surface fixation, and bioactive substance immobilization. *Langmuir* **15**, 1667–1672.
25. Doi, K., Y. Nakayama and T. Matsuda (1996) Novel compliant and tissue-permeable microporous polyurethane vascular prosthesis fabricated using excimer laser ablation technique. *J. Biomed. Mater. Res.* **31**, 27–33.
26. Nakao, H., Y. Nakayama and T. Matsuda (1993) Design concept and construction of a hybrid lamellar keratoprosthesis. *ASAIO J.* **39**, M257–M260.
27. Nakayama, Y. and T. Matsuda (1993) Surface fixation of poly(ethylene glycol) via photodimerization of cinnamate group. *J. Polym. Sci. Polym. Chem. Ed.* **31**, 3299–3305.
28. Szycher, M. (1983) *Biocompatible Polymers, Metals and Composites.* Technomic Publ., Lancaster.
29. Park, J. B. (1984) *Biomaterials Science and Bioengineering.* Plenum Press, New York.
30. Andrade, J. D. (1985) *Surface and Interfacial Aspects of Biomedical Polymers*, Vol. 1 (Edited by J. D. Andrade), p. 1. Plenum Press, New York.
31. Curtis, A. S. G. (1967) Cell adhesion. In *The Cell Surface; Its Molecular Role in Morphogenesis.* Academic Press, London.
32. Okano, T., N. Yamada, H. Sakai and Y. Sakurai (1993) A novel recovery system for cultured cells using plasma-treated polystyrene dishes grafted with poly(*N*-isopropylacrylamide). *J. Biomed. Mater. Res.* **27**, 1243–1251.
33. Bertelson, R. C. (1971) Photochromism. In *Techniques of Chemistry*, Vol. III (Edited by G. H. Brown), pp. 294. Wiley–Interscience, New York.
34. Irie, M. and D. Kungwatchakun (1986) Reversible photostimulated dilation of polyacrylamide gels having triphenylmethane leucoderivatives. *Macromolecules* **19**, 2476.
35. Nakayama, Y. and T. Matsuda (2003) Photo-control of interaction between endothelial cells and photo-cation generatable water-soluble polymers. *J. Control. Release.* (In press)
36. Dilks, A. (1981) X-Ray photoelectron spectroscopy for the investigation of polymeric materials. In *Electron Spectroscopy: Theory, Techniques, and Applications*, Vol. 4 (Edited by A. D. Baker and C. R. Brundle), pp. 277–359. Academic Press, London.
37. Ratner, B. D. and B. J. McElry (1986) Electron spectroscopy for chemical analysis: applications in the biomedical sciences. In *Spectroscopy in the Biomedical Sciences* (Edited by R. M. Gendreau), pp. 107–140. CRC Press, Boca Raton.
38. Neumann, A. W. and R. J. Good (1979) Techniques of measuring contact angles. In *Surface and Colloid Science—Experimental Methods*, Vol. 11 (Edited by R. J. Good and R. R. Stromberg), pp. 31–61. Plenum Publishers, New York.

39. Zisman, W. A. (1964) Relation of the equilibrium contact angle to liquid and solid construction. In *Contact Angle, Wettability and Adhesion, ACS Advances in Chemistry Series*, Vol. 43 (Edited by F. M. Fowkes), pp. 1–51. American Chemical Society, Washington, DC.
40. Rugar, D. and P. Hansma (1990) Atomic force microscopy. *Phys. Today* 43, 23–30.
41. Hansma, P. K., V. B. Elings, O. Marti and C. E. Bracker (1988) Scanning tunneling microscopy and atomic force microscopy: application to biology and technology. *Science* 242, 209–216.
42. Kidoaki, S. and T. Matsuda (1999) Adhesion forces of the blood plasma proteins on self-assembled monolayer surfaces of alkanethiolates with different functional groups measured by an atomic force microscope. *Langmuir* 15, 7639–7646.
43. Determann, H. (1968) *Gel Chromatography: Gel Filtration, Gel Permeation, Molecular Sieves: A Laboratory Handbook*. Springer-Verlag, New York.
44. Yau, W. W., J. J. Kirkland and D. D. Bly (1979) *Modern Size-exclusion Liquid Chromatography: Practice of Gel Permeation and Gel Filtration Chromatography*. Wiley–Interscience Publication, New York.
45. Sharma, C. P. and P. R. Hari (1990) Surface modification of polystyrene-platelet adhesion. *J. Biomater. Appl.* 5, 49–55.
46. Lackie, J. M. (1986) *Cell Movement and Cell Behaviors*. Allen & Unwin, London.
47. van Wachem, P. B., A. H. Hogt, T. Beugeling, J. Feijen, A. Bantjes, J. P. Detmers and W. G. van Aken (1987) Adhesion of cultured human endothelial cells onto methacrylate polymers with varying surface wettability. *Biomaterials* 8, 323–328.
48. Bruil, A., J. G. Terlingen, T. Beugeling, W. G. van Aken and J. Feijen (1992) In vitro leucocyte adhesion to modified polyurethane surfaces. I. Effect of ionizable functional groups. *Biomaterials* 13, 915–925.
49. Harkes, G., J. Feijen and J. Dankert (1991) Adhesion of Escherichia coli on to a series of poly(methacrylates) differing in charge and hydrophobicity. *Biomaterials* 12, 853–860.
50. Goldberg, S., R. J. Doyle and M. Rosenberg (1990) Mechanism of enhancement of microbial cell hydrophobicity by cationic polymers. *J. Bacteriol.* 172, 5650–5654.
51. Watts, K. C. and O. Husain (1984) Optimal use of the cationic polyelectrolyte poly-L lysine in the preparation of cell monolayers for diagnostic cytopathology. *J. Clin. Pathol.* 37, 829–831.
52. van Wachem, P. B., T. Beugeling, J. Feijen, A. Bantjes, J. P. Detmers and W. G. van Aken (1985) Interaction of cultured human endothelial cells with polymeric surfaces of different wettability. *Biomaterials* 6, 403–408.
53. Horbett, T. A., J. J. Waldburger, B. D. Ratner and A. S. Hoffman (1988) Cell adhesion to a series of hydrophilic-hydrophobic copolymers studied with a spinning disc apparatus. *J. Biomed. Mater. Res.* 22, 384–404.
54. Ratner, B. D., T. Horbett, A. S. Hoffman and S. D. Hauschka (1975) Cell adhesion to polymeric materials: implications with respect to biocompatibility. *J. Biomed. Mater. Res.* 9, 407–422.
55. Yamada, K. M., S. S. Yamada and I. Pastan (1976) Cell surface protein partially restores morphology, adhesiveness, and contact inhibition of movement to transformed fibroblasts. *Proc. Natl. Acad. Sci. USA* 73, 1217–1221.
56. Pierschbacher, M. D. and E. Ruoslahti (1984) Variants of the cell recognition site of fibronectin that retain attachment-promoting activity. *Proc. Natl. Acad. Sci. USA* 81, 5985–5988.
57. Hynes, R. O. (1992) Integrins: versatility, modulation, and signaling in cell adhesion. *Cell* 69, 11–25.
58. Lopez, G. P., B. D. Ratner, C. D. Tidwell, C. L. Haycox, R. J. Rapoza and T. A. Horbett (1992) Glow discharge plasma deposition of tetraethylene glycol dimethyl ether for fouling-resistant biomaterial surfaces. *J. Biomed. Mater. Res.* 26, 415–439.

# Coaxial double-tubular compliant arterial graft prosthesis: time-dependent morphogenesis and compliance changes after implantation

Hiromichi Sonoda,[1,2,3] Keiichi Takamizawa,[1] Yasuhide Nakayama,[1] Hisataka Yasui,[2] Takehisa Matsuda[3]
[1]*Department of Biomedical Engineering, National Cardiovascular Center Research Institute, 5-7-1 Fujishirodai, Suita, Osaka 565-8565, Japan*
[2]*Department of Cardiovascular Surgery, Graduate School of Medicine, Kyushu University, 3-1-1 Maidashi, Higashiku, Fukuoka 812-8582, Japan*
[3]*Department of Biomedical Engineering, Graduate School of Medicine, Kyushu University, 3-1-1 Maidashi, Higashiku, Fukuoka 812-8582, Japan*

Received 11 March 2002; revised 10 June 2002; accepted 19 June 2002

**Abstract:** In order to reduce the compliance mismatch between the native artery and the artificial graft, we have developed a coaxial double-tubular compliant graft, using multiply micropored segmented polyurethane (SPU) thin films, which mimics the relationship between the intraluminal pressure and vessel internal diameter (P-D) of the native artery (termed "J" curve). The graft was coaxially assembled by inserting a high-compliance inner tube with a heparin-immobilized photocured gelatin coating layer into a low-compliance outer tube with a photocured hydrophilic polymer coating layer. Twenty-eight coaxial double-tubular compliant grafts were implanted into the canine common carotid arteries in an end-to-end fashion for up to 12 months. The overall patency rate was 86% (24/28), and neither rupture nor aneurysmal formation was observed. A neoarterial wall was formed via transanastomotic and transmural tissue ingrowth, resulting in neoarterial tissue formation on the luminal surface and into the intertubular space of the double-tubular graft, accompanied by mainly myofibroblasts and inflammatory cells in the early stage and endothelialization and collagen-rich extracellular matrices in the late stage of implantation. Surrounding-tissue adhesion with the outer tube was prevented by the hydrophilic polymer coating. Although the J curve of the implanted prototype model was preserved 1 month after implantation, the impaired J curves were observed because of tissue ingrowth and tissue adhesion between the outer surface of the inner tube and the surrounding tissues 3 and 6 months after implantation. At 12 months after implantation, however, the implanted coaxial double-tubular graft exhibited high compliance due to biodegradation of the SPU films. © 2003 Wiley Periodicals, Inc. J Biomed Mater Res 65A: 170–181, 2003

**Key words:** coaxial double-tubular graft; compliance matching; segmented polyurethane; healing process; biodegradation

## INTRODUCTION

Arterial tissues including aorta to arteriole are continuously exposed to a dynamic mechanical force such as perpendicular stress, circumferential stress, and shear stress, which are repeatedly driven by cardiac pulsatile output, and these arteries contribute to efficient forward blood flow to peripheral tissues with minimal energy loss because of their unique biomechanical properties[1,2]: large inflation in the low-pressure regions, gradually reduced inflation in the physiological pressure regions, and little inflation in the high-pressure regions, termed the "J" curve.

On the other hand, artificial grafts such as expanded polytetrafluoroethylene (ePTFE; Gore-tex) and polyester-based (Dacron) grafts, which have been widely used clinically for bypass grafting or the replacement of occluded or aneurysmal arterial tissues, are so stiff that the fabricated tubes show little inflation over full-pressure regions. The patency rate after the implantation of a small-diameter artificial graft has been much lower than that of a medium- to large-diameter artificial graft because of an early stage thrombosis and a

*Correspondence to:* T. Matsuda; e-mail: matsuda@med.kyushu-u.ac.jp
Contract grant sponsor: Promotion Fundamental Studies in Health Science of the Organization for Pharmaceutical Safety and Research (OPSR); contract grant number: 97-15.
Contract grant sponsor: in part by a Grant-in-Aid for Scientific Research from the Ministry of Education, Culture, Sports, Science, and Technology of Japan; contract grant number: A2-12358017 and B2-12470277.

late stage neointimal hyperplasia.[3–6] Among the many factors determining the patency of the small-diameter artificial grafts, the compliance mismatch between the native artery and the artificial grafts has been discussed as a major detrimental factor of graft failure.[1,5,7–10] Thrombus formation and neointimal hyperplasia on the surface of the small-diameter artificial graft become more critical factors for graft failure than those of the medium- to large-diameter artificial graft, because the effective flow area of the small-diameter artificial graft must be much smaller when the same amount of thrombus or neointimal hyperplasia is generated. In addition, the difference in mechanical properties between a native artery and an artificial graft induces hemodynamical flow disturbance and stress concentration near the anastomoses, causing further thrombus formation and neointimal hyperplasia.[1,5,7–10] Therefore, the small-diameter artificial graft essentially requires compliance matching with the native arteries as much as possible.

We reported new design concept based on biomechanical design criteria and fabricated a prototype small-diameter graft of a unique structure[11]: a coaxial double-tubular compliant graft biomimicking the J curve of canine common carotid arteries using micropored segmented polyurethane (SPU) films. SPU has long been used as a material for the artificial heart (e.g., diaphragms or valves), because of proven physical characteristics such as highly flexible elastomer and excellent durability against cyclic stretching. The coaxial double-tubular compliant graft was assembled by inserting the high-compliance inner tube into the low-compliance outer tube (Fig. 1). Upon increasing the intraluminal hydrodynamic pressure, the inner tube inflates markedly in the low-pressure regions (Fig. 1, phase A to B), and after the inner tube comes in contact with the outer tube (Fig. 1, phase B), both tubes inflate together gradually in the high-pressure regions (Fig. 1, phase C). This mechanical property mimicks the J curve of the native artery. The wall thickness, diameter and pore density (relative area of micropores), which are the principal parameters determining the pressure-dependent diameter change, were adjusted to meet the design criteria of the graft (target vessel was canine carotid arteries: inner diameter, 4.0 mm; averaged from eight arteries) and were 50 μm, 4.5 mm, and 35.1% for the inner tube, and 100 μm, 5.5 mm, and 15.0% for the outer tube, respectively (Fig. 2). This fabricated coaxial double-tubular graft exhibited the J curve mimicking that of target canine carotid arteries. The transition point was set within the physiological pressure range (100 mmHg).

In this article, the surface processing aiming at reduced thrombus formation on the luminal surface of the inner tube in the early stage of implantation and prevention of tissue-mediated adhesion between the inner and outer tubes and between the outer tube and the surrounding tissues, was conduced by photochemical grafting. Upon implantation into canine carotid arteries, morphogenesis and compliance changes were investigated. The perspective of the coaxial double-tubular graft and the shortcomings of the current technology were discussed.

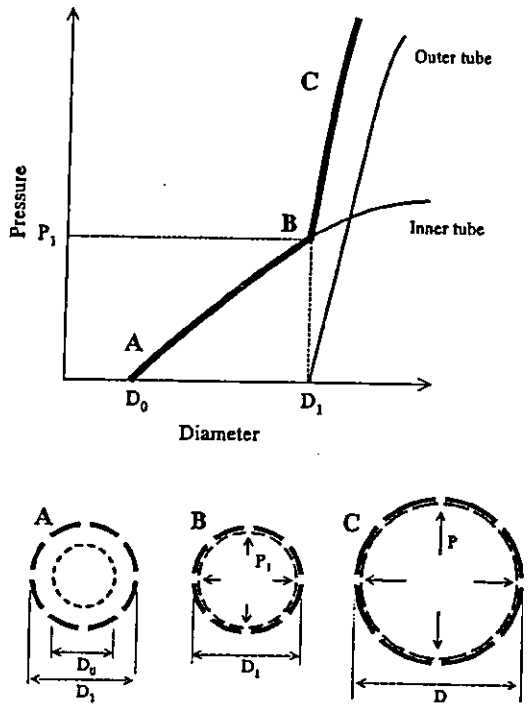


**Figure 1.** Design concept of the coaxial double-tubular compliant graft. Top: the conceptual pressure-diameter relationship of the coaxial double-tubular graft. Bottom: the short-axis views of the coaxial double-tubular graft, depending on the intraluminal pressure. Phase A: at zero pressure; phase B: at $P_1$ (contact phase); phase C: at given P (high-pressure regions). The inner tube inflates rapidly in the low-pressure regions (phase A to B). After the inner tube comes in contact with the outer tube (phase B), both tubes inflate together gradually (phase C).

## MATERIALS AND METHODS

### Fabrication of coaxial double-tubular compliant graft

The design criteria and the detailed fabrication procedures of the coaxial double-tubular compliant graft were reported previously.[11] Briefly, our graft was assembled by inserting a high-compliance inner tube into a low-compliance outer tube. The materials used were multiply micropored segmented polyurethane thin films (Cardiomat 610, Zeon Kasei Co., Ltd., Tokyo, Japan). It is claimed by the manufacture that Cardiomat 610, a segmented poly(urethane-ether) was prepared from poly(teramethylene glycol), 1,4-diphenyl methane diisocyanate and 1,4-butanediol

| | Diameter | Pore Density | Wall Thickness |
|---|---|---|---|
| Inner tube | 4.5 mm | 35.1% | 50 μm |
| Outer tube | 5.5 mm | 15.0% | 100 μm |

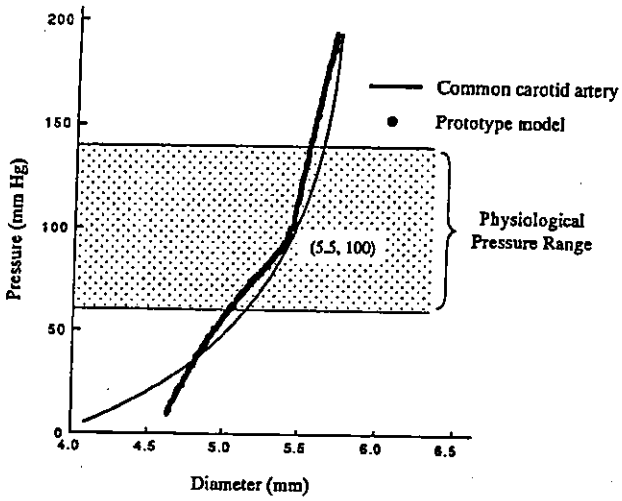


Figure 2. Design criteria and pressure-diameter relationship of the prototype model of the coaxial double-tubular graft. The pressure-diameter relationships of the prototype model matched well with that of the common carotid artery in the intermediate and higher pressure regions, and the transition point was set within the physiological pressure range.

(chain extender). The material descriptions including dimensions are listed in Figure 2 and shown in Figure 3.

A surface coating was applied to the graft using a photografting technique previously developed by us. The outer and inner surfaces of the inner tube were coated with a mixed aqueous solution of 2 wt % photoreactive gelatin [benzophenone-derivatized gelatin: number of benzophenone groups is 29.9 per gelatin molecule (molecular weight: $9.5 \times 10^4$)] and 1 wt % heparin (Wako Pure Chemicals Inc., Osaka, Japan) and subsequently photocured by ultraviolet (UV) light irradiation from a mercury arc lamp (H-400P, Toshiba, Tokyo, Japan; $\lambda > 270$ nm; intensity, 0.14 mW/cm$^2$).[12–15] The outer and inner surfaces of the outer tube were coated with 1% aqueous solution of a photoreactive hydrophilic polymer, poly(*N,N*-dimethylacrylamide-*co*-m-azidostyrene) (azidostyrene content: 10 mol %; molecular weight: $2.0 \times 10^4$) and subsequently photocured by UV light irradiation.[16]

## Animal models

Twenty-eight coaxial double-tubular compliant grafts were bilaterally implanted into the common carotid arteries of 14 adult mongrel dogs (average weight, 28.5 ± 2.2 kg; range, 25–35 kg, Table I). All animals received care according to the "Principles of Laboratory Animal Care" (formulated by the National Society for Medical Research) and the "Guide for the Care and Use of Laboratory Animals" (NIH publication no. 86-23, revised 1985).

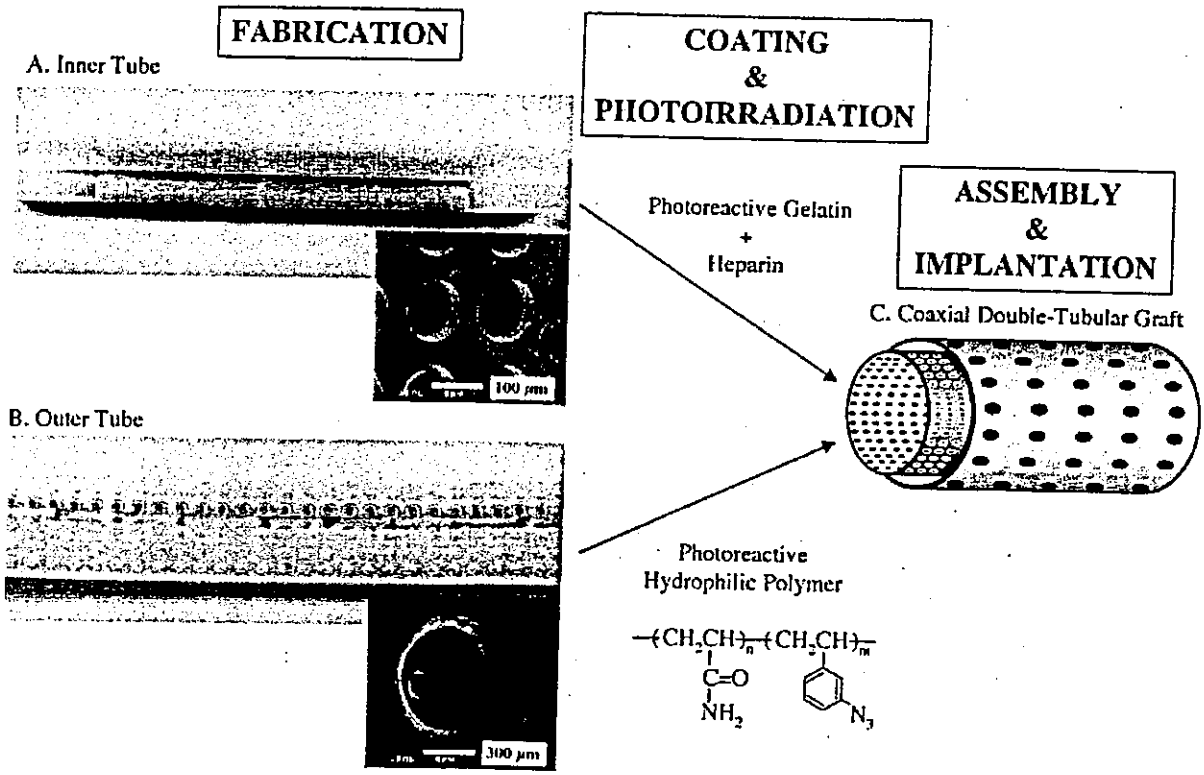


Figure 3. Fabrication process of the coaxial double-tubular graft. The inner and outer tubes were fabricated and coated separately, and the coaxial double-tubular graft was assembled by inserting the inner tube into the outer tube.

TABLE I
Patency as a Function of Implantation Period

| Implantation Period (month) | Body Weight (kg) | No. of Patent Grafts/ No. of Implanted Grafts |
|---|---|---|
| 1 | 28.5 ± 1.0 | 7/8 (88%) |
| 3 | 29.7 ± 3.5 | 6/6 (100%) |
| 6 | 28.0 ± 1.7 | 5/6 (83%) |
| 12 | 28.0 ± 2.7 | 6/8 (75%) |
| Average | 28.5 ± 2.2 | 24/28 (86%) |

## Graft implantation

General anesthesia was induced by injection of intramuscular ketamine (Ketaral 50, Sankyo Co., Ltd., Tokyo, Japan; 15 mg/kg) and intravenous pentobarbital (Nembutal, Dainippon Pharmaceutical Co., Ltd., Osaka, Japan; 10 mg/kg) and maintained by intermittent injection of pentobarbital. Bilateral para-tracheal incisions were made along the trachea, and both common carotid arteries were dissected, which yielded a segment approximately 10 cm in length. After intravenous injection of heparin (Novo Heparin, Novo Nordisk Pharmaceuticals, Copenhagen, Denmark; 100 U/kg), the arteries were crossclamped 20 mm away from the anastomoses, and a segment 30 mm long was resected. The coaxial double-tubular graft was interposed by means of end-to-end anastomosis (Fig. 4). The anastomoses of the inner tube were constructed with 12 interrupted 7-0 polypropylene sutures (Nespilene, Azwell Co., Ltd., Osaka, Japan) on each side, and the outer tube that was placed outside of the inner tube over the anastomosis was roughly fixed to the adventitia of the adjacent native artery. Neither antiplatelet nor anticoagulant agents were administered except for the intraoperative heparin injection.

## Histological examination

All grafts were fixed *in situ* with 20% formaldehyde and 4% glutaraldehyde except for the grafts subjected to measurement of the compliance (P-D relationship), which were fixed after the measurement. Specimens for light microscopic examination were stained with hematoxylin-eosin, Masson's trichrome, and Elastica van Gieson to observe the time-dependent changes of neoarterial structure and wall thickness of the grafts after implantation. For immunohistochemical staining, the antibodies against the smooth muscle α-actin (1A4, DAKO Corp., Glostrup, Denmark) and the von Willebrand factor (A082, DAKO Corp.) were used to identify the smooth muscle cells (SMCs) and the endothelial cells (ECs), respectively. Specimens for scanning electron microscopic observation were postfixed with 1% osmium tetroxide, dehydrated in graded series of ethanol, critical point dried, and sputter-coated with osmium to identify the endothelial ingrowth of the luminal surface of the grafts. The surfaces of the SPU materials of the retrieved outer tubes were also observed using a scanning electron microscope (SEM: JSM-6301F, JEOL, Tokyo, Japan).

## Measurements of P-D relationship and compliance

The P-D relationships of the retrieved grafts with adjacent arteries at 1, 3, 6, and 12 months after implantation were measured using a digital X-ray imaging system and a pressure transducer as previously reported.[17] Briefly, one end of a vessel segment was cannulated to a fixed stainless steel connector for pressure loading and the other to a sliding connector, and the vessel was restored to *in situ* length in a bath filled with Krebs-Ringer solution held at 37°C. The vessel was gradually inflated with a pressurized contrast medium (Iomeron 350, Eisai Co., Ltd., Tokyo, Japan) using a syringe pump, recording the intraluminal pressures from 0 to ~200 mmHg. An X-ray digital fluoro-imaging system (series 9600, OEC Medical Systems Inc., Salt Lake City, UT) was used for obtaining the intraluminal radiographs of the vessel, and real-time digital images were recorded on a digital videocassette tape. The P-D relationships at the middle portion of the grafts were measured using an NIH Image software (Version 1.59, public domain software). The details of the procedure were described in our previous article.[17]

Compliance changes were evaluated with the stiffness parameter (β value) determined from the following equation[18,19]:

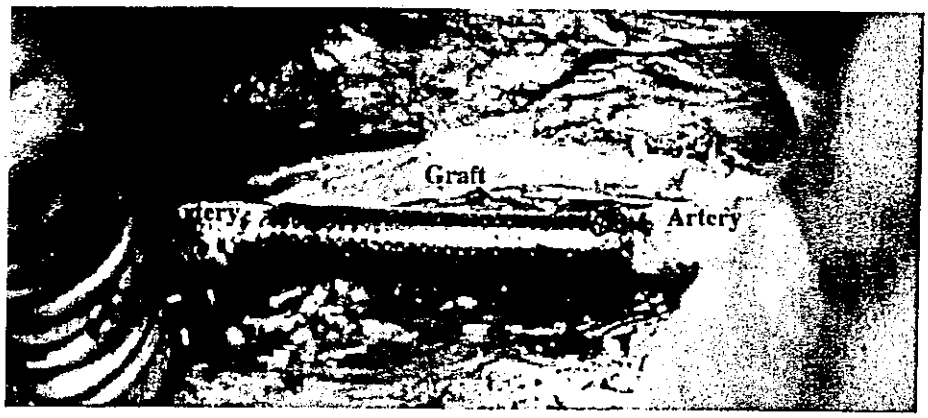


Figure 4. Operative findings of the coaxial double-tubular grafts. The grafts were implanted into the canine common carotid arteries in an end-to-end fashion.

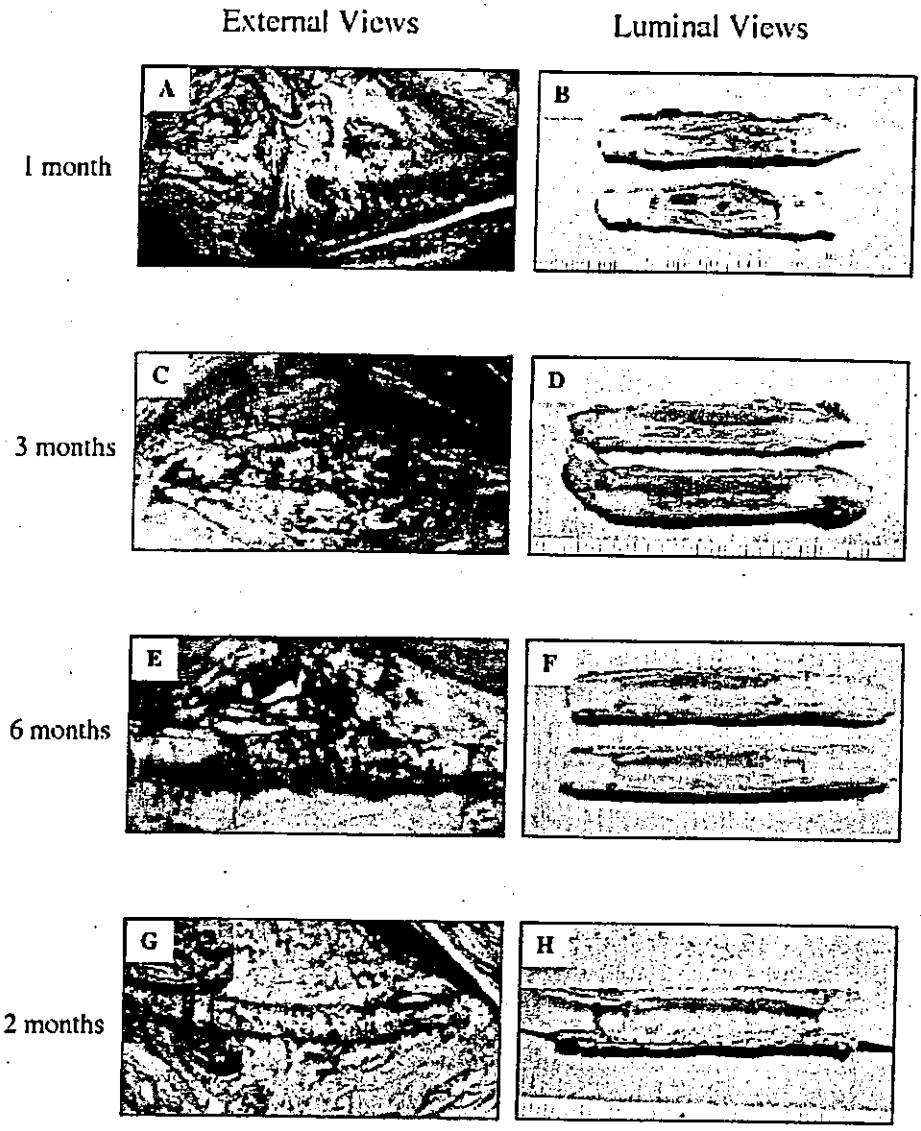


**Figure 5.** The external and luminal views of the grafts after implantation.

$$\ln (P/Ps) = \beta(D/Ds - 1) \quad (1)$$

where *Ps* and *Ds* are the standard intraluminal pressure (100 mmHg in this study) and the external diameter at *Ps*, respectively. *P* is the intraluminal pressure and *D* is the external diameter at *P*.

## RESULTS

The fabrication procedure of double-tubular graft is schematically shown in Figure 3. The diameters of inner and outer tubes were 4.5 and 5.5 mm, respectively. For both tubes, the inner and outer surfaces were photografted with a respective photoreactive substance. The inner tube was coated with a photocured heparin-immobilized gelatin layer, and the outer tube was photografted with a hydrophic polymer, poly(*N,N*-dimethylacrylamide) partially derivatized with a photoreactive group (phenylazide). Both surface processing technologies and materials were described in our previous articles.[12–16] These grafts were bilaterally implanted into canine common carotid arteries up to 12 months. Figure 4 shows a photograph of the surgical operation. When anastomosed and blood-circulated, the periodic cycles of inflation and deflation of the graft were noted, indicating that pulsatile blood flow was taking place in the implanted graft.

### Patency and macroscopic appearance

Twenty-four of the 28 grafts were patent at the moment of explantation (overall patency rate: 86%;

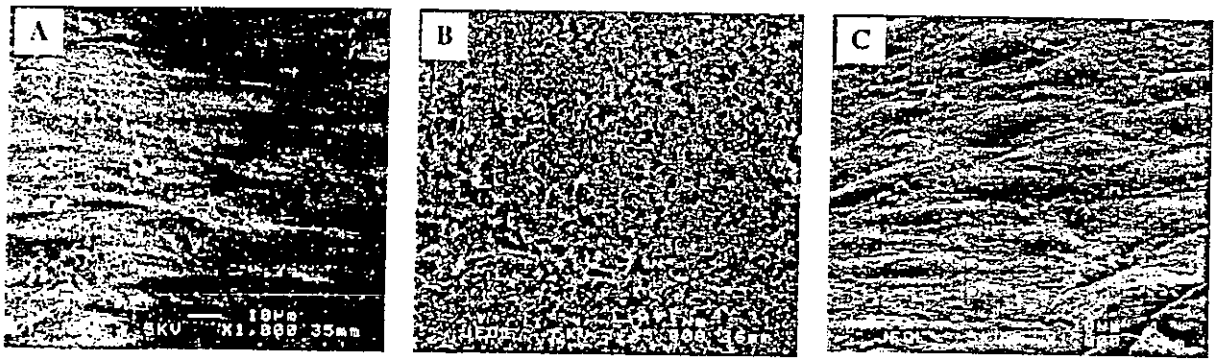


Figure 6. Scanning electron microscopic findings of the luminal surface of the implanted graft. (A) Anastomosis portion at 1 month after implantation (original magnification, ×1000). (B) Middle portion at 3 months after implantation (original magnification, ×5000). (C) Middle portion at 6 months after implantation (original magnification, ×1000).

Table I). Figure 5 shows the external and luminal views of the implanted graft at various times. Neither rupture nor aneurysmal formation was observed even at 12 months after implantation. Tissue adhesion around the graft was most massive at 1 month after implantation [Fig. 5(A)], but the degree of adhesion reduced gradually with the implantation period [Fig. 5(C,E,G)]. The outer tube photografted with a hydrophilic polymer could be retrieved easily without adhesion between the inner and outer tubes in all observation periods. The intertubular space between the inner and outer tubes was filled with ingrowth tissues that migrated from the tissues surrounding the graft or from the host arteries.

In the luminal views, thrombus formation was observed at 1 and 3 months after implantation [Fig. 5(B,D)]. At 6 and 12 months after implantation, the luminal surface was almost covered with glistening and milky-white neointima with little thrombus and neointimal hyperplasia [Fig. 5(F,H)].

### Implantation-period-dependent morphogenesis

SEM observation shows that the ECs infiltrated sequentially from both proximal and distal stumps of the host artery into the graft surface beyond the anastomoses [Fig. 6(A)]. The endothelializing front was positioned at ~3 mm from the anastomoses at 1 month after implantation, and at ~7 mm at 3 months after implantation. At 1 and 3 months after implantation, the luminal surface of the graft where ECs were not found was covered with the thrombus or fibrin [Fig. 6(B)]. At 6 months after implantation, however, the luminal surface was completely covered with ECs [Fig. 6(C)].

The neoarterial wall was reconstructed by tissue ingrowth from the arterial stumps and from the surrounding tissues through the micropores of the grafts. The tissue ingrowth inside the inner tube and the tissue ingrowth into the intertubular space between the inner and outer tubes were defined here as the neointima and the neomedia, respectively. At 1 month after implantation, the neointima and the neomedia near the anastomosis were filled with myofibroblast-rich cells and inflammatory cells [Fig. 7(A), 8, and 9(A)], and fresh thrombus was attached to the luminal surface of the middle portion of the graft [Figs. 7(E) and 9(E)]. At 3 months after implantation, the neointima and the neomedia near the anastomosis began to be replaced with collagen-rich extracellular matrices [Figs. 7(B) and 9(B)], although fibrin was attached to the luminal surface of the middle portion of the graft [Figs. 7(F) and 9(F)]. At 6 months after implantation, the neointima and the neomedia were almost replaced with extracellular matrices, and the cellular components were localized at the luminal side of the neointima [Figs. 7(C,G) and 9(C,G)]. At 12 months after implantation, well-aligned smooth muscle cell layers, the thickness of which were approximately 50 to 80 μm, were observed beneath the intima [Figs. 7(D,H), 9(D,H), and 10(A,B)], although elastic fibers were not observed among those layers [Fig. 10(C)]. Also, the luminal surface of the neointima was fully covered with ECs [Fig. 10(D)].

Figure 11 shows the time-dependent change of wall thickness. The neointimal wall thickness at para-anastomosis of the grafts at 3 months after implantation was the largest (512 ± 41 μm) and decreased at 6 and 12 months after implantation (414 ± 54 μm at 6 months, and 313 ± 48 μm at 12 months). The neointimal wall thickness in the middle portion of the grafts became larger with time, reaching approximately 315 ± 30 μm at 12 months after implantation [Fig. 11(A)]. On the other hand, the neomedial wall thicknesses at para-anastomosis of the grafts were significantly larger than those in the middle portion in all observation periods except that at 3 months [Fig. 11(B)].

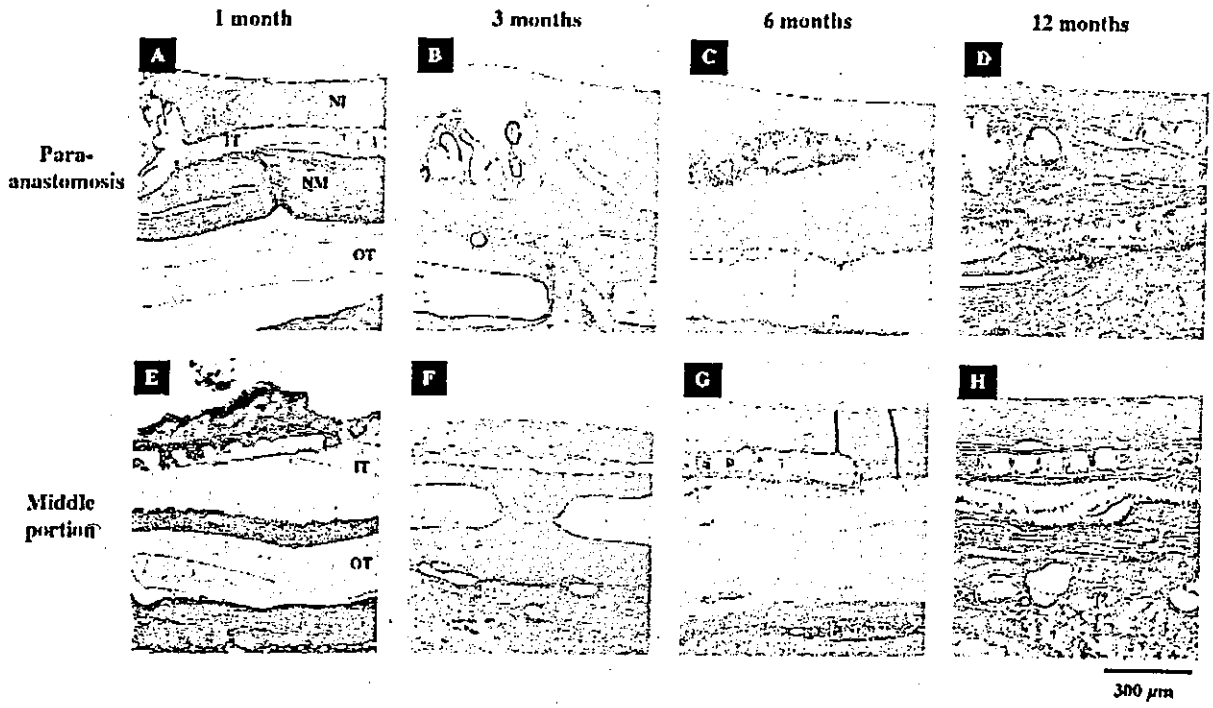


Figure 7. Longitudinal sections at the para-anastomosis and the middle portion of the grafts after implantation. The sections were stained with hematoxylin-eosin. IT, inner tube; OT, outer tube; NI, neointima; NM, neomedia. Original magnification, ×40.

### Compliance changes and material deterioration

The P-D relationships after implantation are shown in Figure 12. The P-D relationship at 1 month after implantation exhibited the J curve but became steeper at 3 and 6 months after implantation. The J curve was restored only within the low-pressure regions. However, the J curve was observed again at 12 months after implantation. This curve closely resembled that of the native arteries: large inflation in the low-pressure regions and gradual inflation in the high-pressure regions. The stiffness parameter (β value), calculated from Equation (1), is also shown in Figure 12: the β value of the preimplanted graft was 9.2, which was

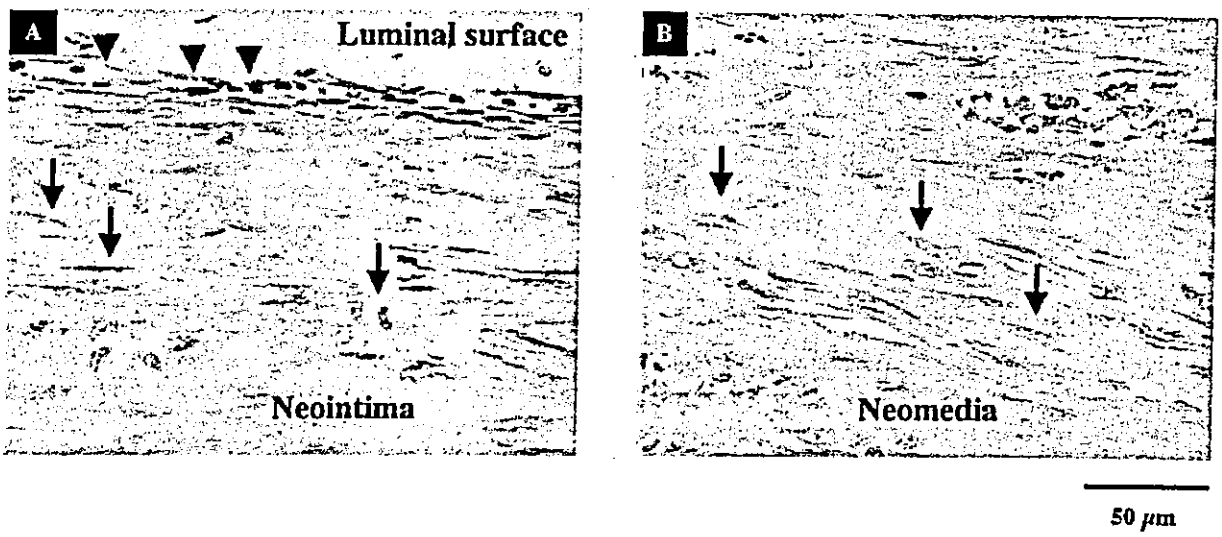


Figure 8. Microscopic findings at the para-anastomosis of the graft at 1 month after implantation (hematoxylin-eosin staining). Arrows and arrowheads indicate myofibroblasts and inflammatory cells, respectively. Original magnification, ×400.

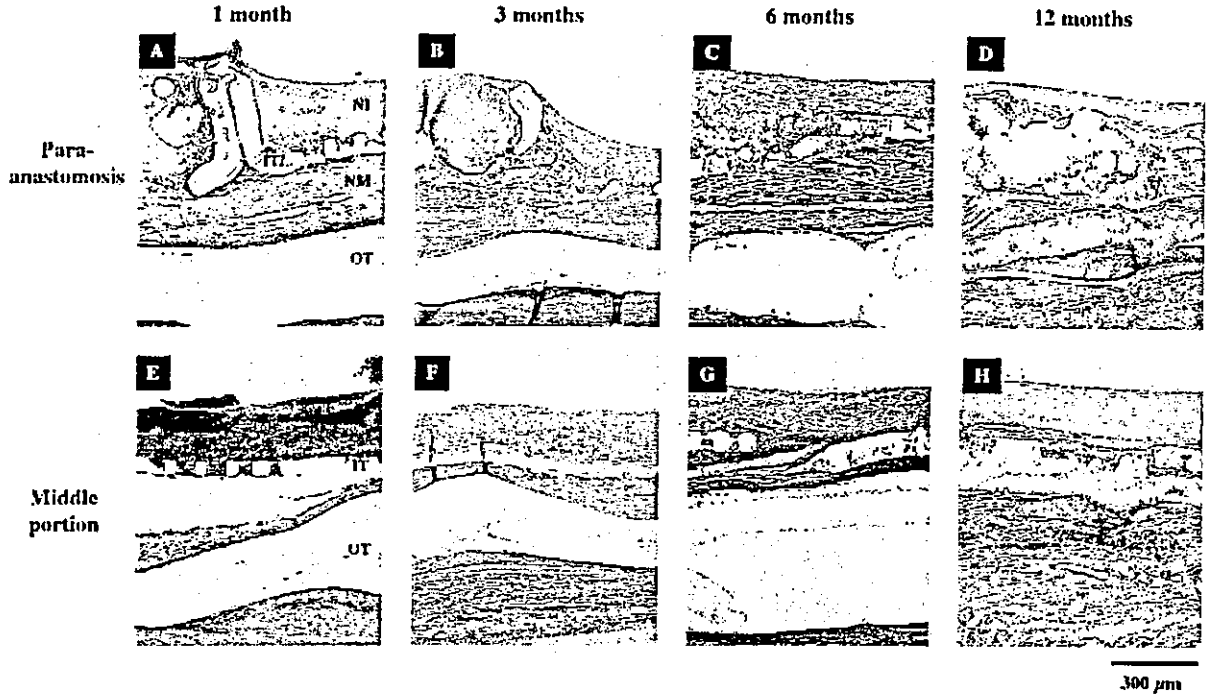


Figure 9. Longitudinal sections at the para-anastomosis and the middle portion of the grafts after implantation. The sections were stained with Masson's trichrome. IT, inner tube; OT, outer tube; NI, neointima; NM, neomedia. Original magnification, ×40.

comparable to that of the native artery but with longer implantation periods; the β value increased to 51.4 at 6 months after implantation but decreased to 19.6 at 12 months after implantation.

SEM observations of the surfaces of the material (SPU) are shown in Figure 13. The surface and edge of the fabricated micropores before implantation were fairly smooth [Fig. 13(A)]. However, the surface gradually became rougher with time [Figs. 13(B–D)], and many deep cracks were observed around the fabricated micropores at 12 months after implantation [Fig. 13(D)], strongly indicating that the SPU film degraded with time, resulting in the loss of integrity leading to the decrease of mechanical strength of the SPU film of the tube.

## DISCUSSION

Despite much effort and various approaches as well as numerical attempts to develop vitally functioning small-diameter artificial grafts for many years, a majority of the research works have shown only the partial improvements including surface-biocompatible modification or the quality of the graft material, and only a few research groups have continued to develop novel small-diameter artificial grafts in terms of material, surface, and structural designs.[20–22]

The structural components of native arteries are mainly cellular elements (SMCs and ECs) and connective tissue elements (elastic and collagenous fibers). Among these components, the latter elements contribute to the mechanical strength of the native artery and the unique mechanical property of the native artery (termed J curve): an artery easily inflates in the low-pressure regions (0 to ~60 mmHg), moderately inflates in the physiological pressure regions (~60–140 mmHg), and hardly inflates in the high-pressure regions (approximately >140 mmHg). The single synthetic elastomeric tube made of SPU generally exhibits an "inverse J" curve in the P-D relationship due to creep characteristics of the elastomeric film, which occur under high stretching conditions. To overcome this problem, our conceptual design and fabrication technology are based on the coaxial double-tubular graft, that was assembled by two different types of elastomeric tubes: the inner tube has high-compliance and the outer tube has low-compliance, and theoretically and experimentally this type of graft mimicked the J curve, as shown in Figure 2.

Although the J curve in the P-D relationship was realized by the optimal selections of material, structural, and fabrication parameters as described in our previous article, one potential problem that remains to be solved is the tissue adhesion between the inner and outer tubes upon tissue ingrowth and that be-

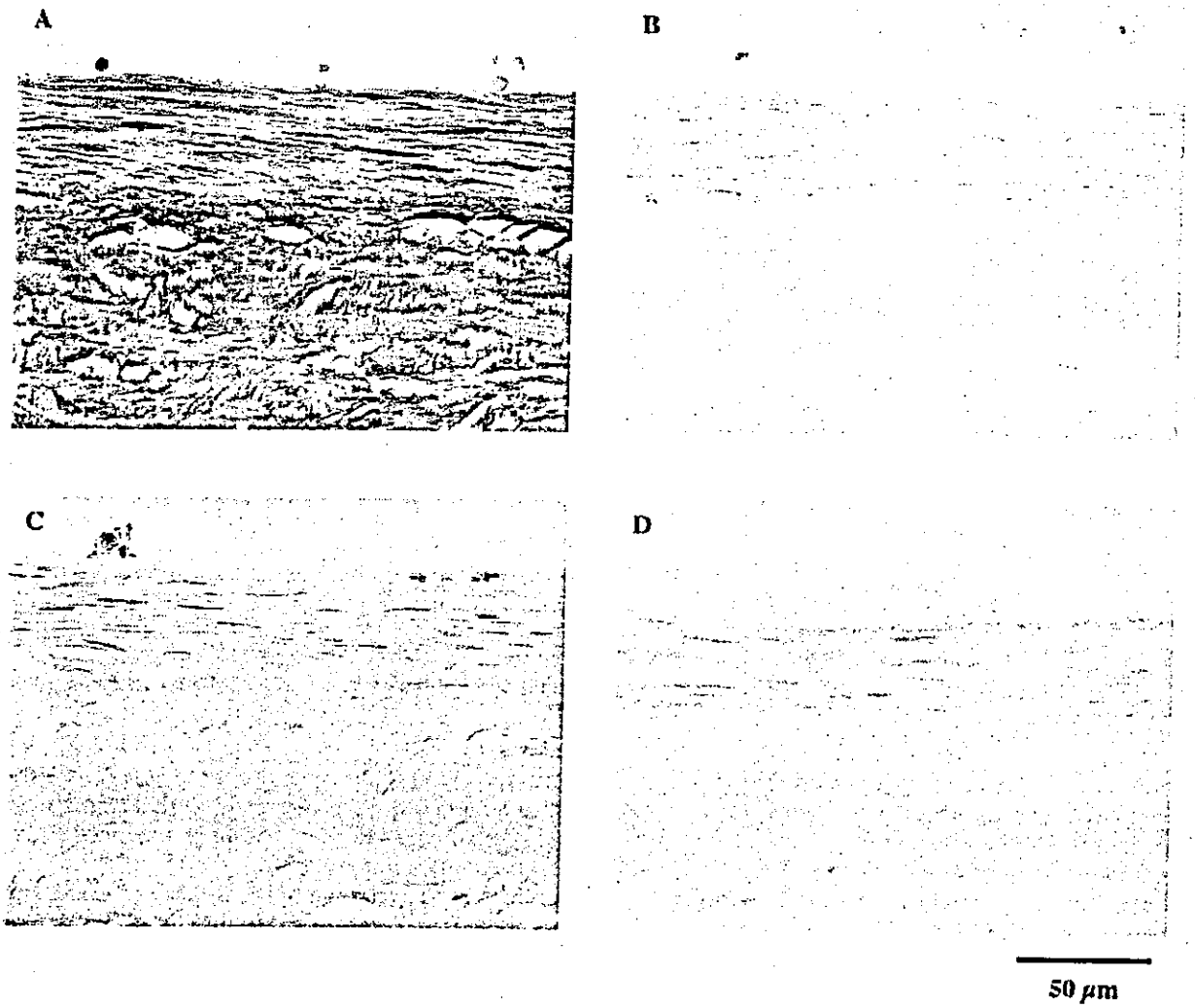


**Figure 10.** Longitudinal sections at the middle portion or the graft at 12 months after implantation. (A) Masson's trichrome staining. (B) Staining for smooth muscle α-actin. (C) Elastica van Gieson's staining. (D) Staining for von Willebrand factor.

tween the outer tube and the surrounding tissue. If these occur during the implantation period, the two tubes would unify to behave as a single tube for the former case or show considerably reduced compliance for the latter case. To circumvent or solve these problems, we performed surface photoprocessing of these tubes, and this led to long-term patency and restoration of compliance. The coating material was

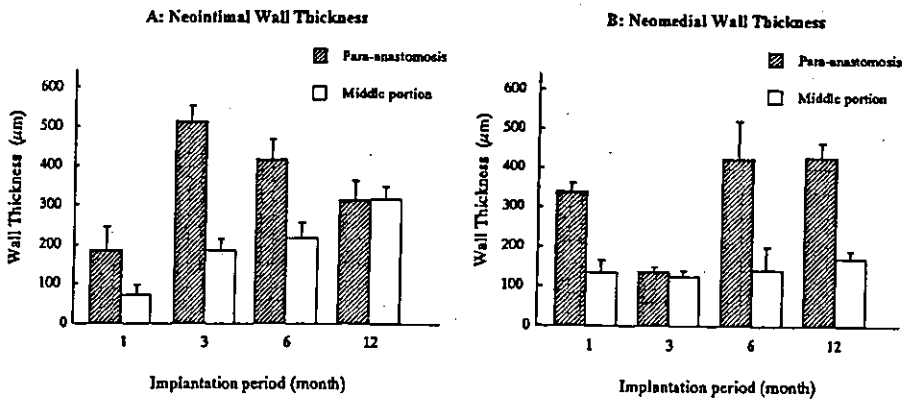


**Figure 11.** Time-dependent changes of neointima (A) and neomedia (B) at the para-anastomosis and the middle portion of the grafts after implantation.